Selective MS Screening Reveals a Sex Pheromone in *C. briggsae* and Species-Specificity in Indole Ascaroside Signalling.

Chuanfu Dong, Franziska Dolke and Stephan H. von Reuss*

ELECTRONIC SUPPORTING INFORMATION

[a] *Max Planck Institute for Chemical Ecology, Department of Bioorganic Chemistry, Hans-Knoell Strasse 8, D-07745 Jena, Germany.E-mail: svonreuss@ice.mpg.de.*

Figure S1: ESI-HR-MS/MS analysis of synthetic icas#9 (4). a) ESI-(+)-HR-MS spectrum of icas#9 shows a cluster of quasi molecular ion adducts along with an intensive fragment ion signal for $C_{15}H_{16}NO_4$ derived from in source collision induced dissociation (ISCID); b) ESI-(+)-HR-MS/MS spectrum of the $[M+NH_4]^+$ adduct confirms that the $C_{15}H_{16}NO_4$ fragments originates from icas#9 via collision induced fragmentation (CID); c) identity of the icas-specific $C_{15}H_{16}NO_4$ fragment ion was further corroborated by MS/MS which gave fragment ions for $[C_9H_8NO_2]^+$ and $[C_9H_6NO]^+$ for the indole-3-carboxylic acid moiety; d) ESI-(-)-HR-MS/MS spectrum of the $[M-H]^-$ ion shows loss of the indole carbonyl moiety to afford the ascr#9 ion $C_{11}H_{19}O_6$ as previously reported (von Reuss et al., 2012).

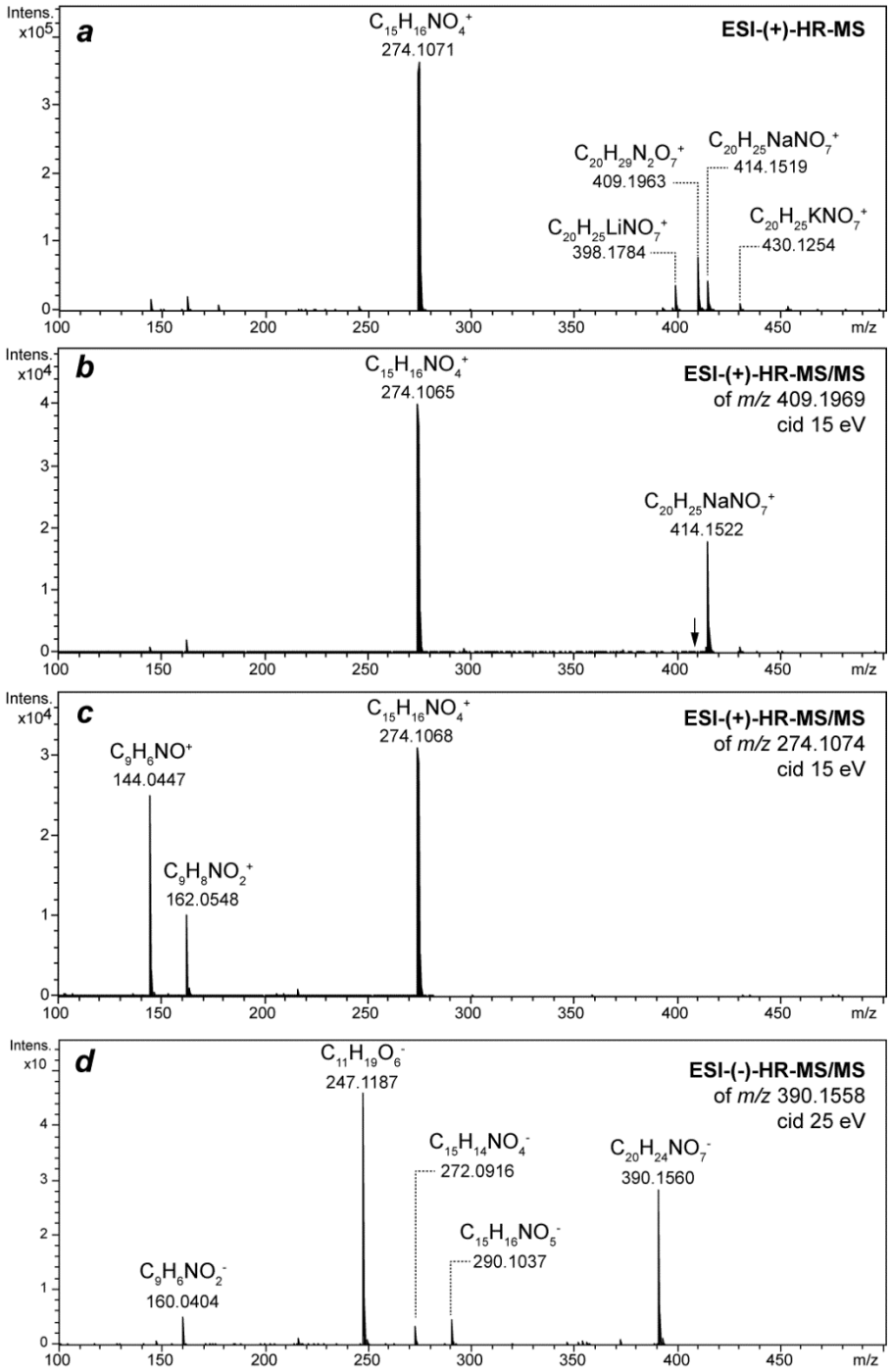

Figure S2: ESI-HR-MS/MS analysis of synthetic icas#9 methyl ester (5). a) ESI-(+)-HR-MS spectrum of icas#9 methyl ester shows a cluster of quasi molecular ion adducts along with an intensive fragment ion signal for $C_{15}H_{16}NO_4$ derived from in source collision induced dissociation (ISCID); b) ESI-(+)-HR-MS/MS spectrum of the $[M+NH_4]^+$ adduct confirms that the $C_{15}H_{16}NO_4$ fragments originates from icas#9 Me via collision induced fragmentation (CID); c) identity of the icas-specific $C_{15}H_{16}NO_4$ fragment ion was further corroborated by MS/MS which gave fragment ions for $[C_9H_8NO_2]^+$ and $[C_9H_6NO]^+$ for the indole-3-carboxylic acid moiety; d) ESI-(-)-HR-MS/MS spectrum of the $[M-H]^-$ ion shows loss of the side-chain moiety to afford a fragment ion for $C_{15}H_{14}NO_4$.

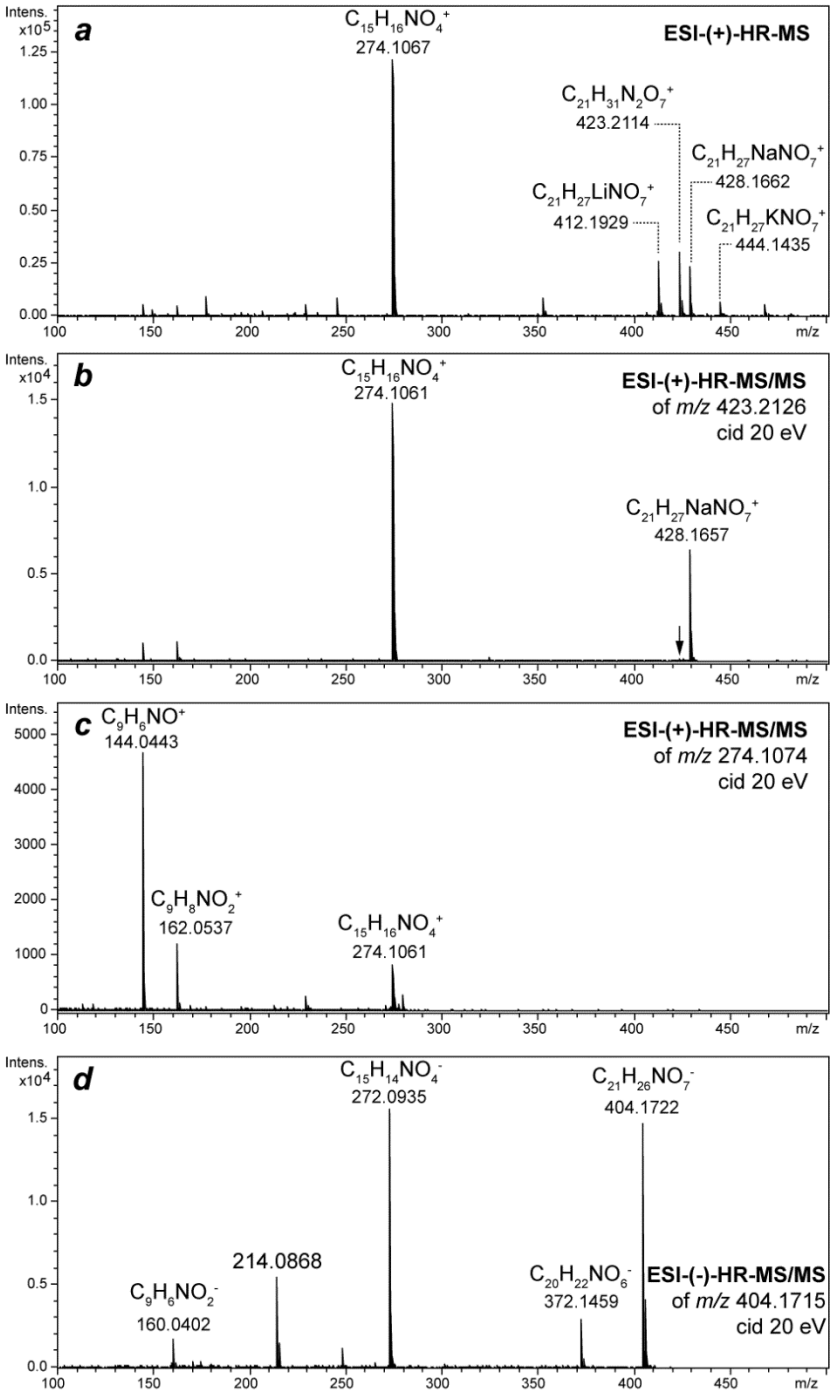

Figure S3: ESI-HR-MS/MS analysis of icas#2 (6) from *C. briggsae*. a) ESI-(+)-HR-MS spectrum of icas#2 shows quasi molecular ion adducts along with an intensive fragment ion signal for $C_{15}H_{16}NO_4$ derived from in source collision induced dissociation (ISCID); b) ESI-(+)-HR-MS/MS spectrum of the $[M+NH_4]^+$ adduct confirms that the $C_{15}H_{16}NO_4$ fragments originates from icas#2 via collision induced fragmentation (CID); c) identity of the icas-specific $C_{15}H_{16}NO_4$ fragment ion was further corroborated by MS/MS which gave fragment ions for $[C_9H_8NO_2]^+$ and $[C_9H_6NO]^+$ for the indole-3-carboxylic acid moiety; d) ESI-(-)-HR-MS/MS spectrum of the $[M-H]^-$ ion shows loss of the side-chain moiety to afford a fragment ion for $C_{15}H_{14}NO_4$.

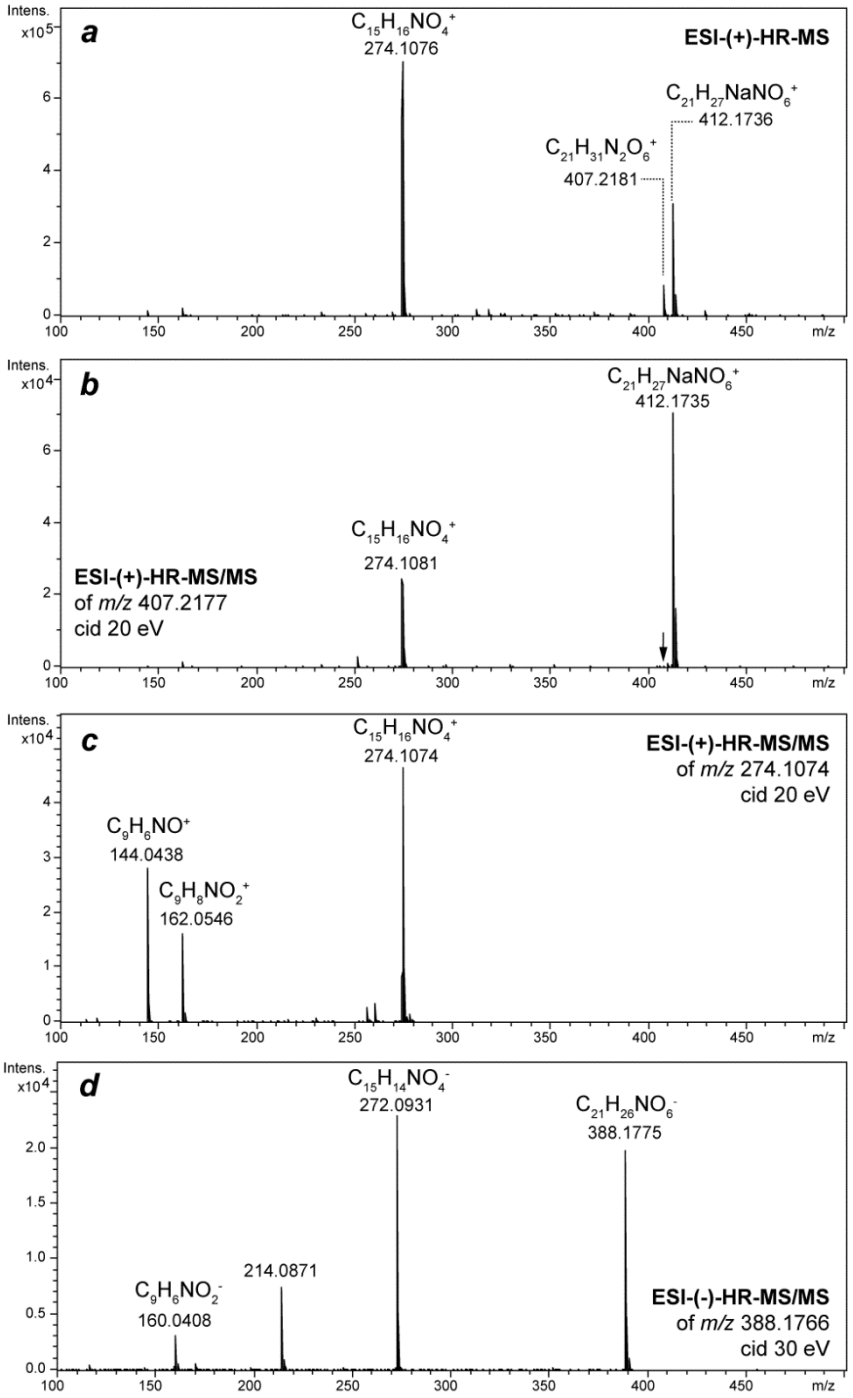

Figure S4: ESI-HR-MS/MS analysis of icas#6.2 (7) from *C. briggsae*. a) ESI-(+)-HR-MS spectrum of icas#6.2 shows quasi molecular ion adducts along with an intensive fragment ion signal for $C_{15}H_{16}NO_4$ derived from in source collision induced dissociation (ISCID); b) ESI-(+)-HR-MS/MS spectrum of the $[M+NH_4]^+$ adduct confirms that the $C_{15}H_{16}NO_4$ fragments originates from icas#2 via collision induced fragmentation (CID); c) identity of the icas-specific $C_{15}H_{16}NO_4$ fragment ion was further corroborated by MS/MS which gave fragment ions for $[C_9H_8NO_2]^+$ and $[C_9H_6NO]^+$ for the indole-3-carboxylic acid moiety; d) ESI-(-)-HR-MS/MS spectrum of the $[M-H]^-$ ion shows loss of the side-chain moiety to afford a fragment ion for $C_{15}H_{14}NO_4$.

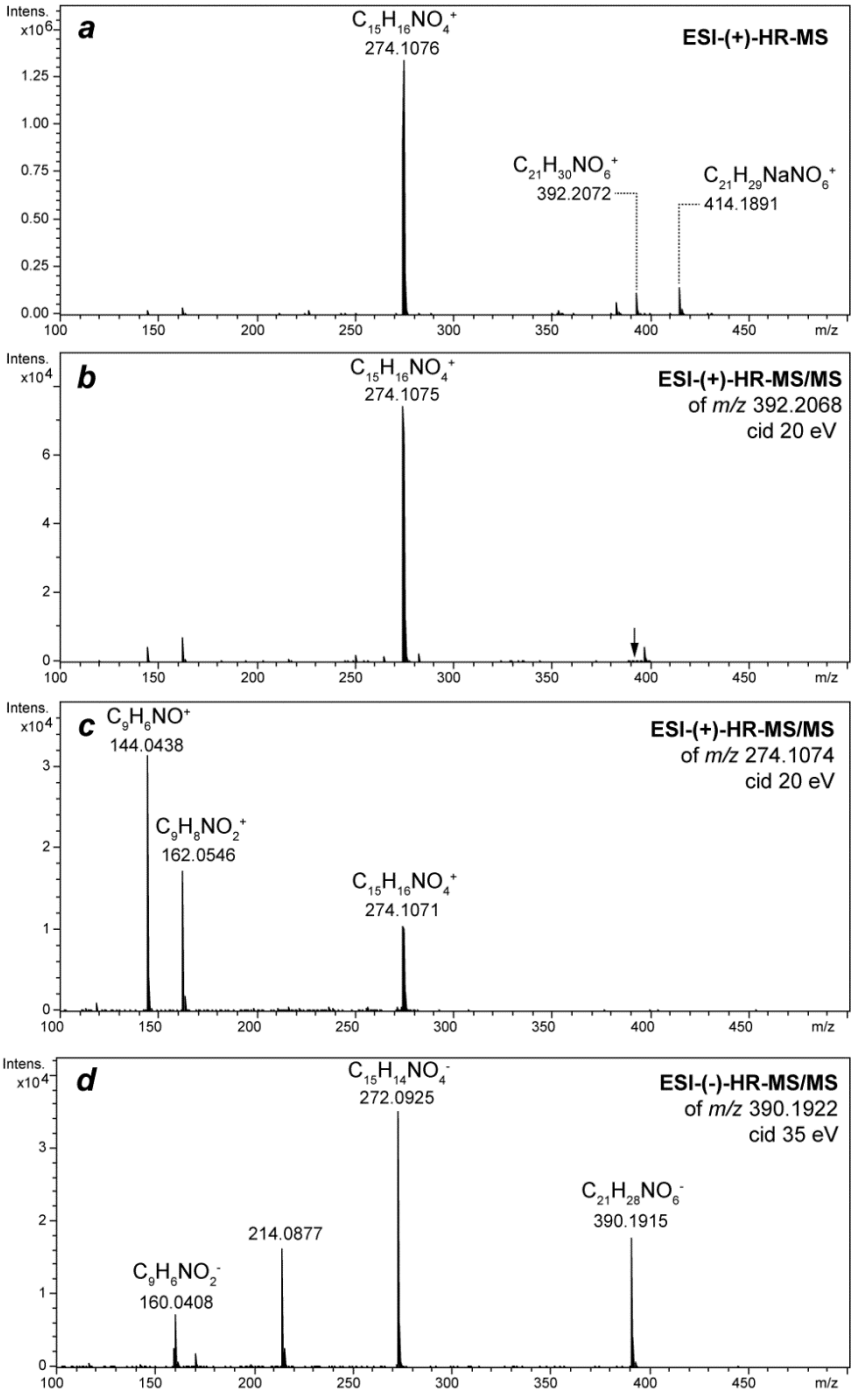

Figure S5: Relative composition of indole ascarosides in 13 wild type isolates of the cosmopolitan *C. briggsae* including (A) tropical strains, (B) temperate strains, and (C) outgroup strains,[16,17] demonstrates that production of icas#2 (6) and icas#6.2 (7) is highly conserved (Cx = sidechain length).

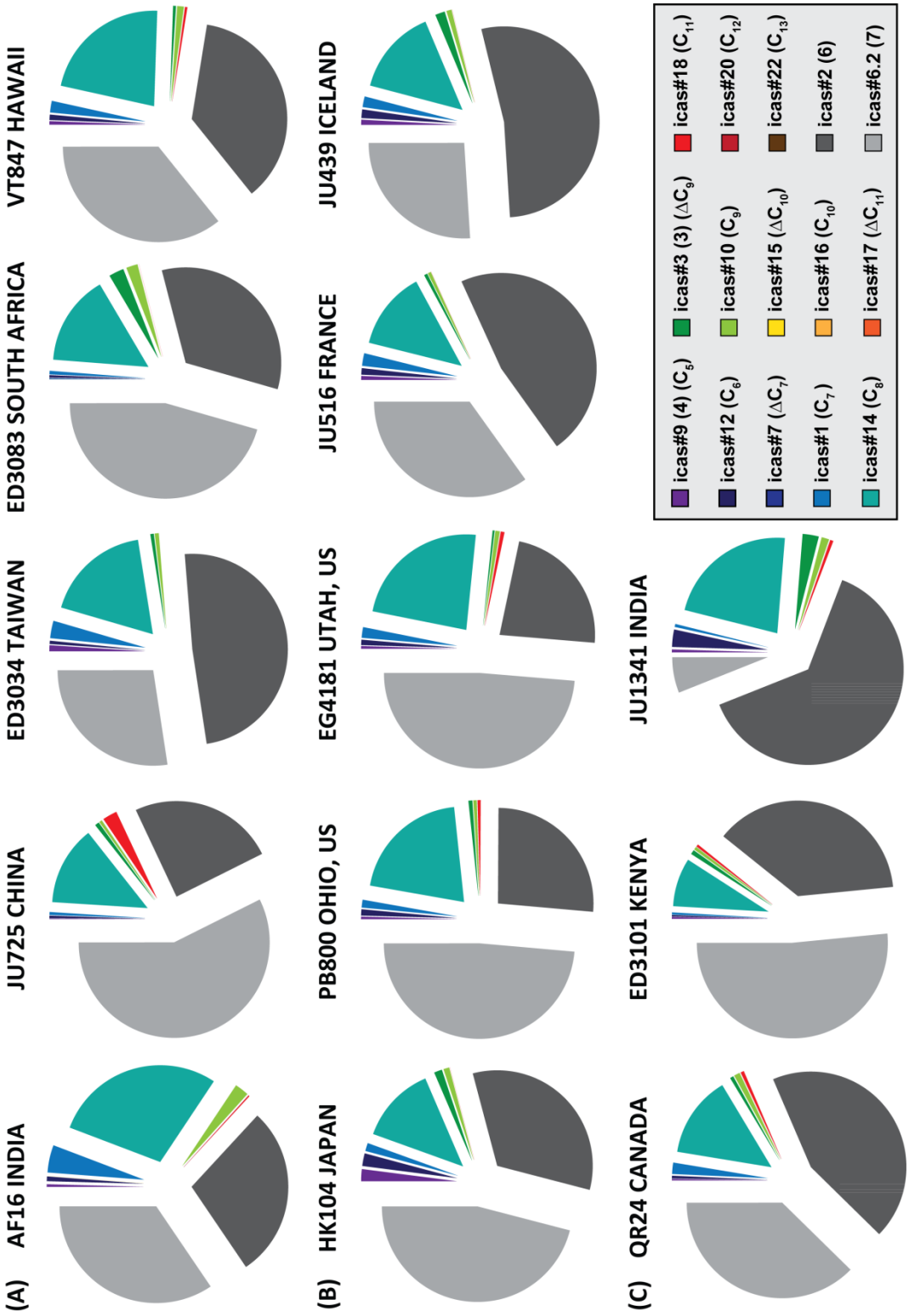

Figure S6: Chemical correlation of natural (*S*)-icas#6.2 (7) isolated from the *C. briggsae* (AF16) *exo*-metabolome with synthetic (*R*)-icas#6.1 (14) and icas#2 (6) of known stereochemistry. **(a)** Sodium borohydride reduction of synthetic icas#2 (**6**) afforded a 1:1 mixture of diastereoisomeric (*R*)-icas#6.1 (**14**) and (*S*)-icas#6.2 (**7**) which could not be separated by HPLC. **(b)** The partial ^{1}H NMR spectrum of the diastereoisomeric mixture of (*R*)-icas#6.1 (**14**) and (*S*)-icas#6.2 (**7**) obtained by $NaBH_4$ reduction of 34 µg icas#2 (**6**) was identical to **(c)** the partial ^{1}H NMR spectrum of a 1:1 mixture of 8.5 µg synthetic (*R*)-icas#6.1 (**14**) and 8.5 µg of the natural icas#6.2 (**7**) isolated from the *C. briggsae* (AF16) *exo*-metabolome, demonstrating that the natural material has a (*S*)-configuration; **(d)** Partial ^{1}H NMR spectrum of 8.5 µg synthetic (*R*)-icas#6.1 (**14**); **(e)** Partial ^{1}H NMR spectrum of 8.5 µg natural (*S*)-icas#6.2 (**7**) isolated from *C. briggsae* strain AF16.

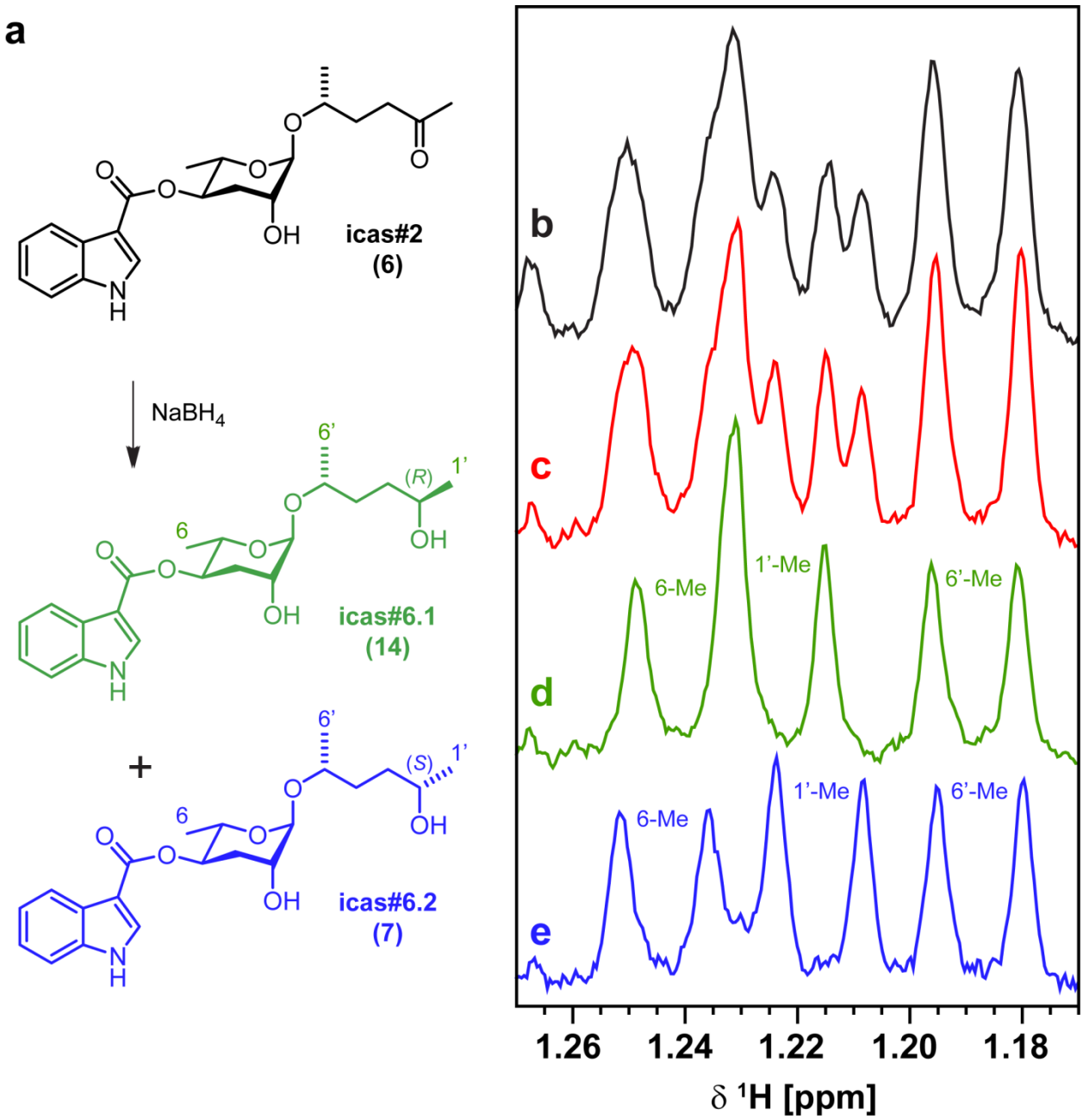

Figure S7: Detection of ascr#2 and ascr#6 in *C. briggsae*. HPLC-ESI-(+)-HR-MS ion traces corresponding to ascr#2 (*m/z* 269.29222 $[M+Na]^+$ for $C_{12}H_{22}NaO_5$) and ascr#6 (*m/z* 271.30822 $[M+Na]^+$ for $C_{12}H_{24}NaO_5$) in the *C. briggsae* (AF16) *exo*-metabolome extract.

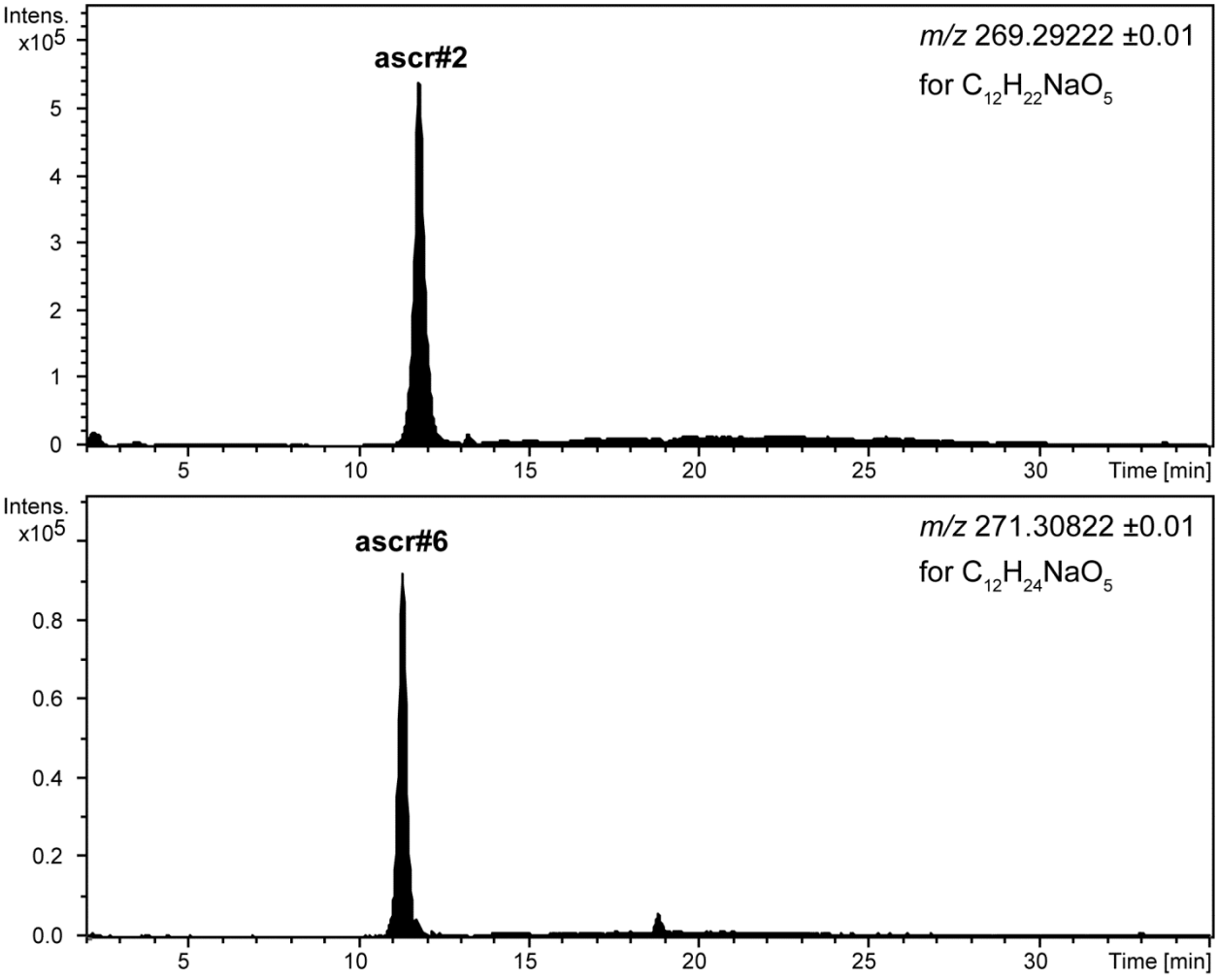

Figure S8: Male specific response to icas#2 (6) and icas#6.2 (7) in *C. briggsae* HK104. *C. briggsae* males from the temperate strain HK104 from Japan spent significantly longer times in regions conditioned with 10 fmol icas#2 or 1 fmol (*S*)-icas#6.2 (±1SD, One-way ANOVA with Dunett's posttest, *p<0.001; n = 10 worms each).

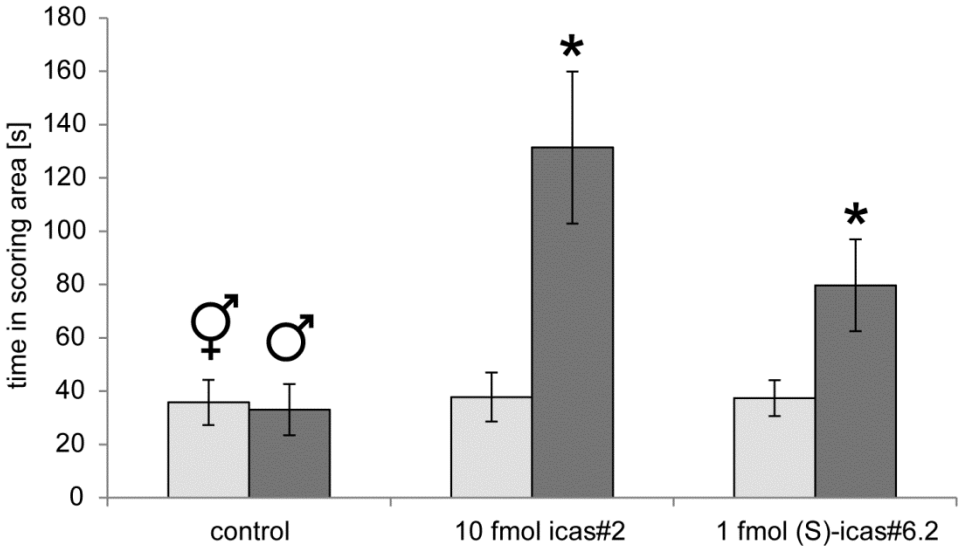

Figure S9: Behavioral activity of icas#6.2 depends on the (*S*)-stereochemistry. Holding assay with *C. briggsae* (AF16) males shows significant attraction to 1 fmol of the natural (*S*)-icas#6.2 isolated from the *C. briggsae exo*-metabolome whereas the diastereoisomeric (*R*)-icas#6.1 displays no activity at any of the concentrations tested (±1SD, One-way ANOVA with Dunett's posttest, *p<0.001; n = 10 worms each).

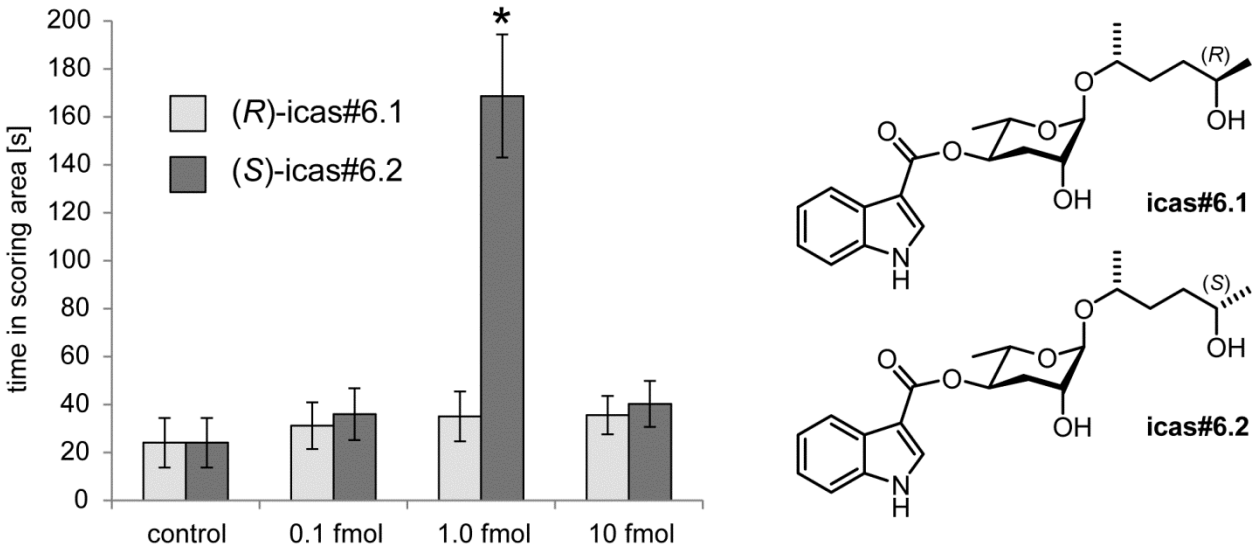

Figure S10: Concentrations of dominating indole ascarosides. Quantitative LC-MS analysis of *exo*-metabolome extracts from nematode cultures grown for 15 days under identical conditions using authentic standards indicated that concentrations of the most prominent indole ascaroside components ranges from low nM to pM concentrations (±1SD).

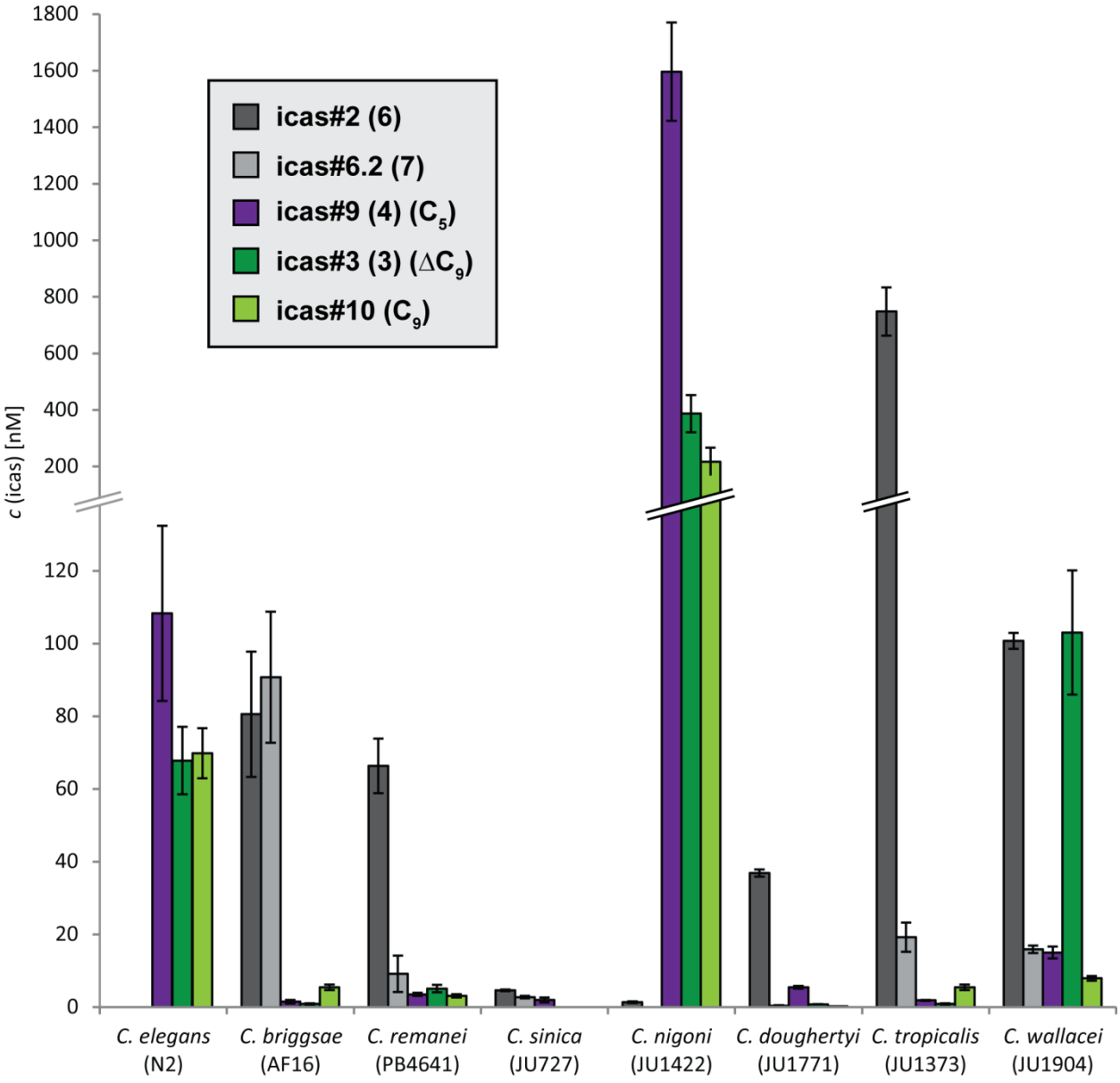

Figure S11a: Increase of holding times in regions conditioned with 1-10000 fmol indole ascarosides (±1SD, One-way ANOVA with Dunett's posttest, *p<0.001).

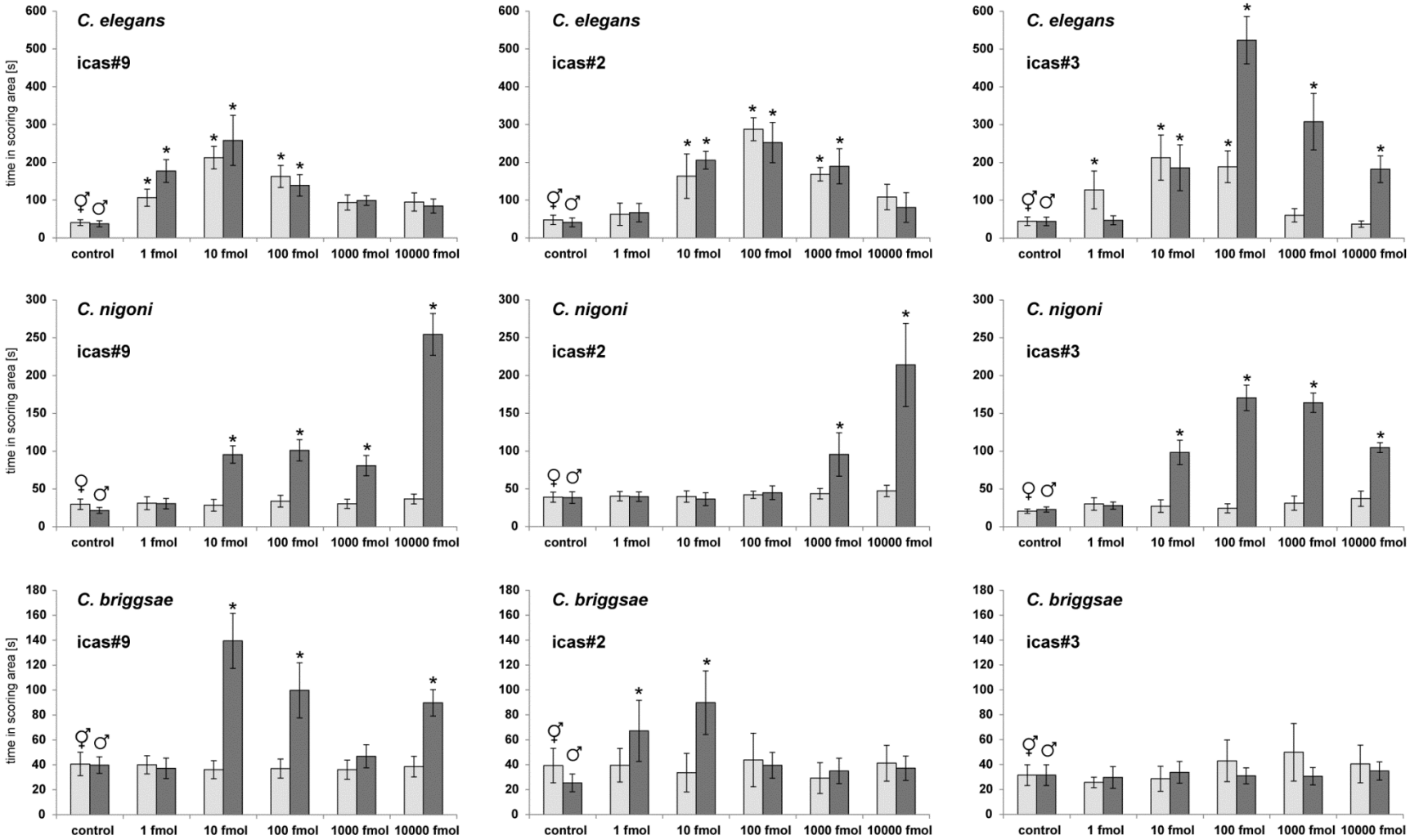

Figure S11b: Increase of holding times in regions conditioned with 1-10000 fmol indole ascarosides (±1SD, One-way ANOVA with Dunett's posttest, *p<0.001).

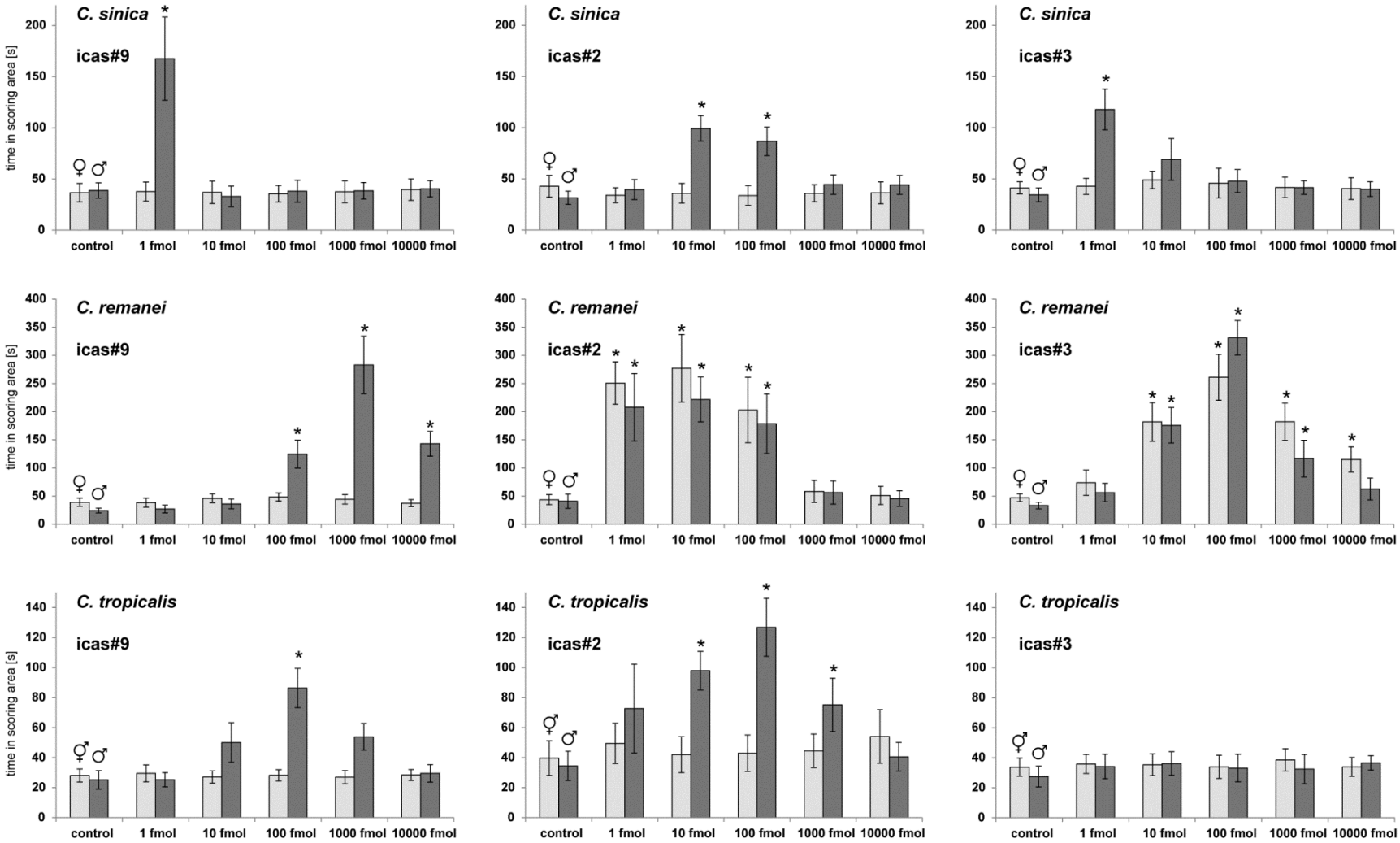

Figure S11c: Increase of holding times in regions conditioned with 1-10000 fmol indole ascarosides (±1SD, One-way ANOVA with Dunett's posttest, *p<0.001).

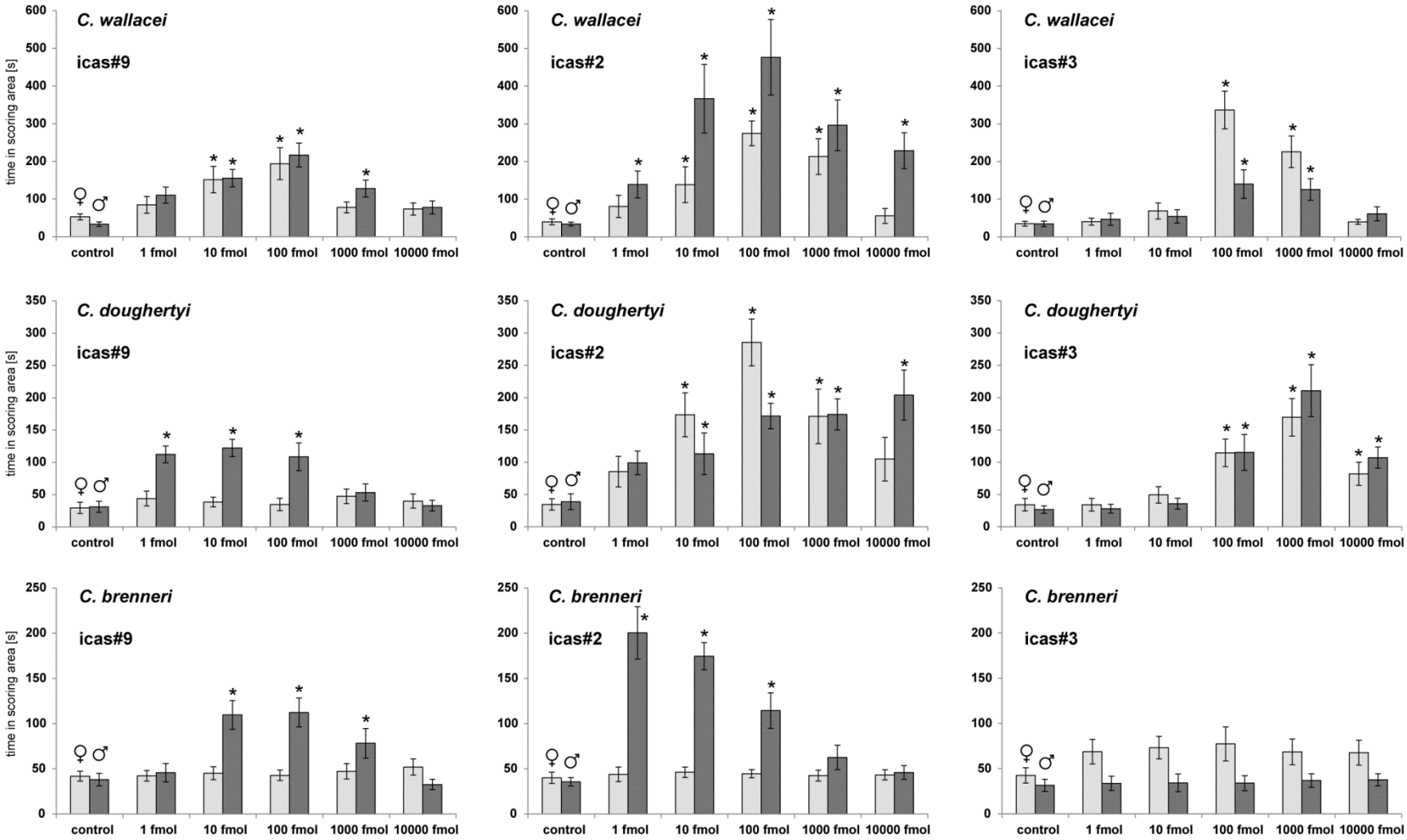

Figure S12: *dqf*-COSY spectrum of indole ascaroside containing SPE fraction (in CD_3OD) from the *C. briggsae* AF16 *exo*-metabolome.

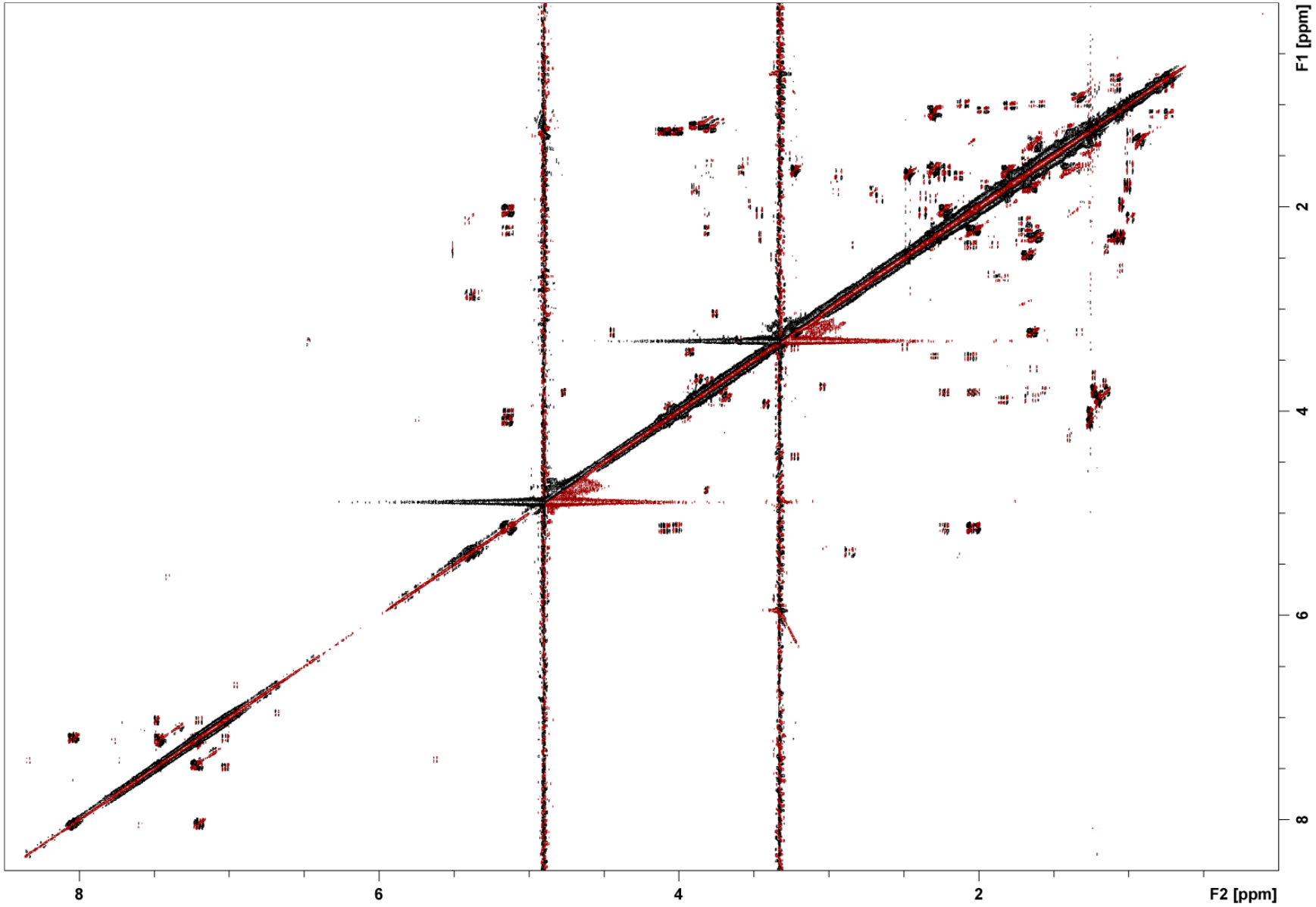

Figure S13: ^{1}H NMR spectrum of icas#2 (**6**) (in CD_3OD) isolated from the *C. briggsae* AF16 *exo*-metabolome.

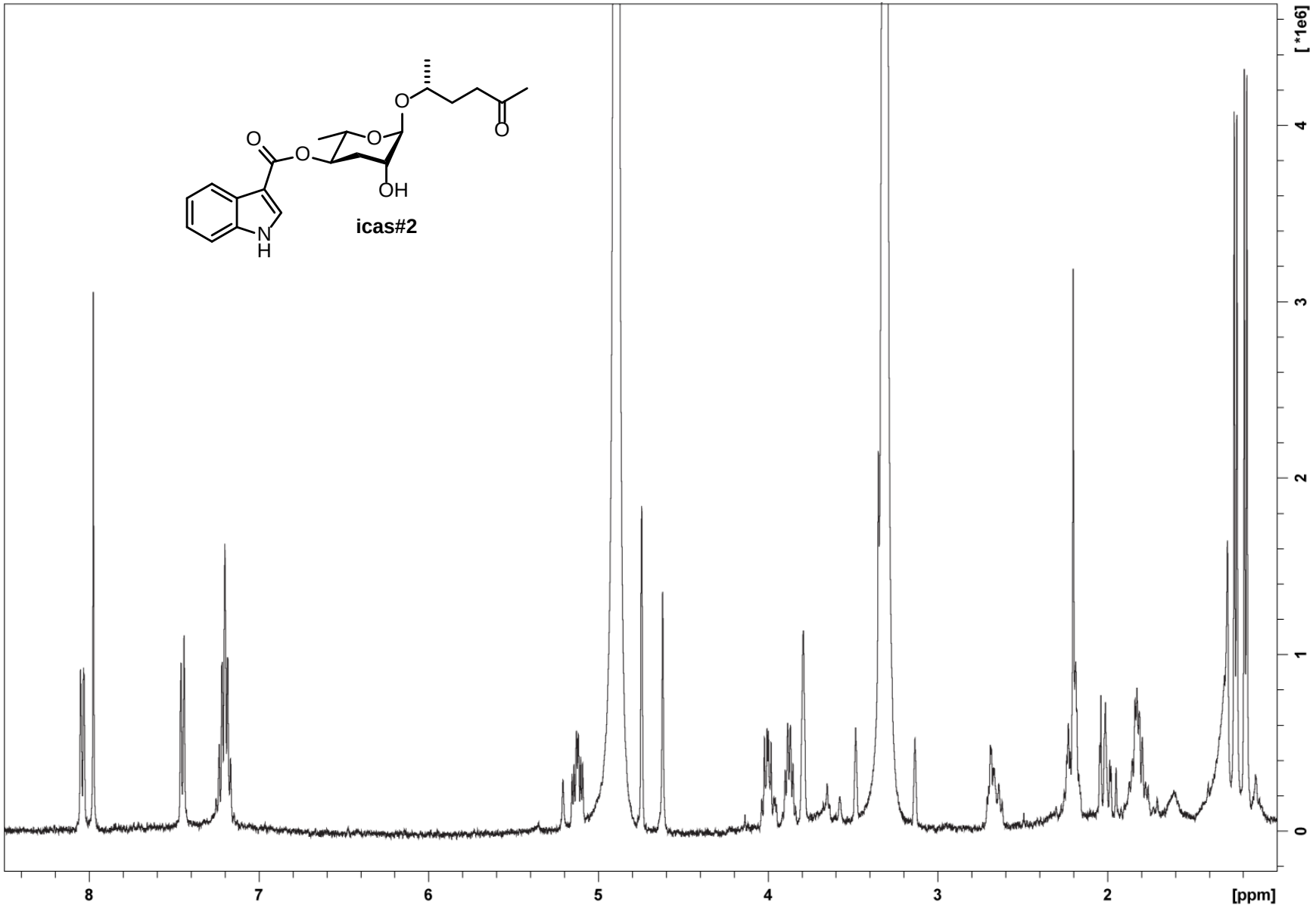

Figure S14: *dqf*-COSY spectrum of icas#2 (**6**) (in CD_3OD) isolated from the *C. briggsae* AF16 *exo*-metabolome.

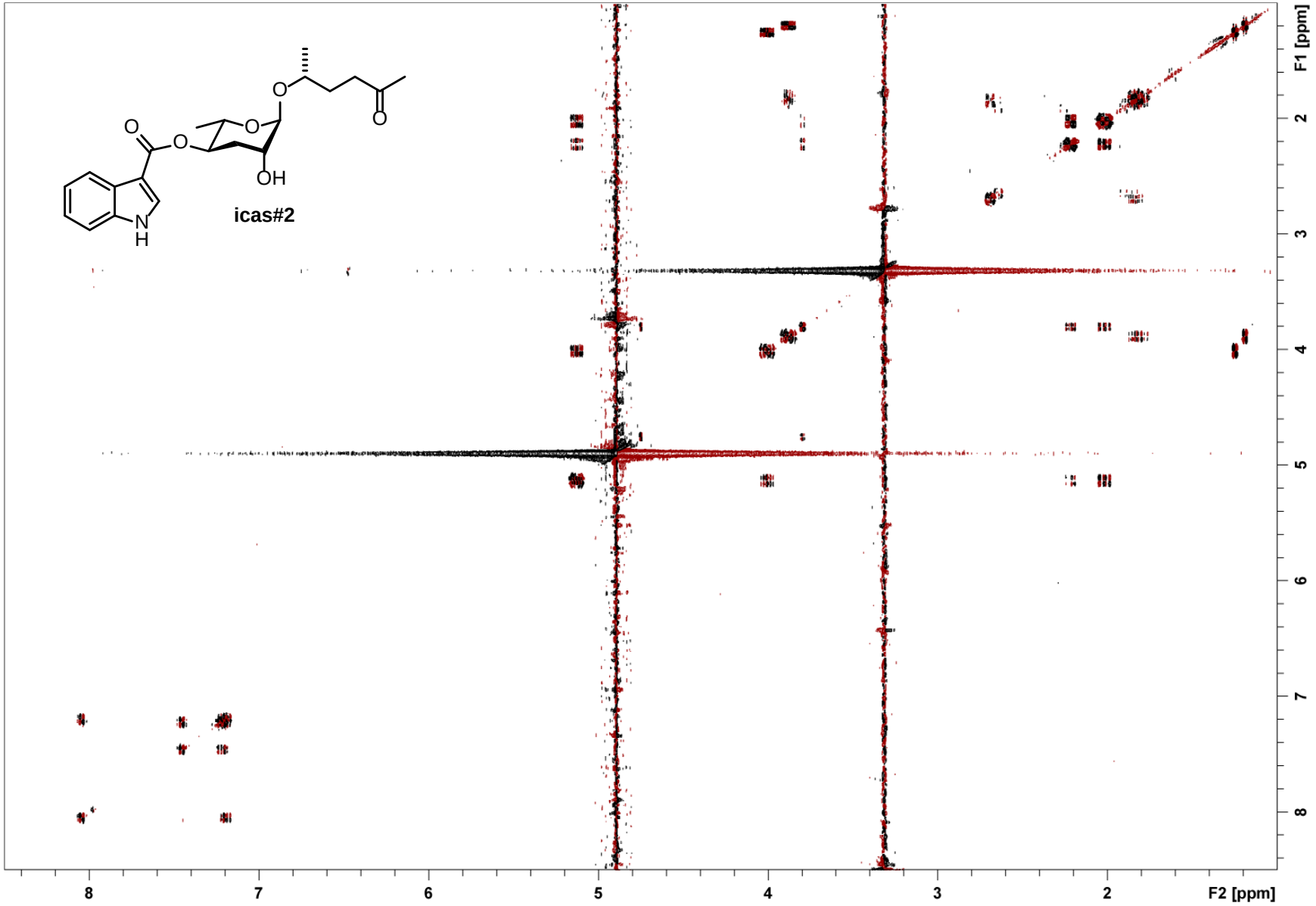

Figure S15: HSQC spectrum of icas#2 (**6**) (in CD_3OD) isolated from the *C. briggsae* AF16 *exo*-metabolome.

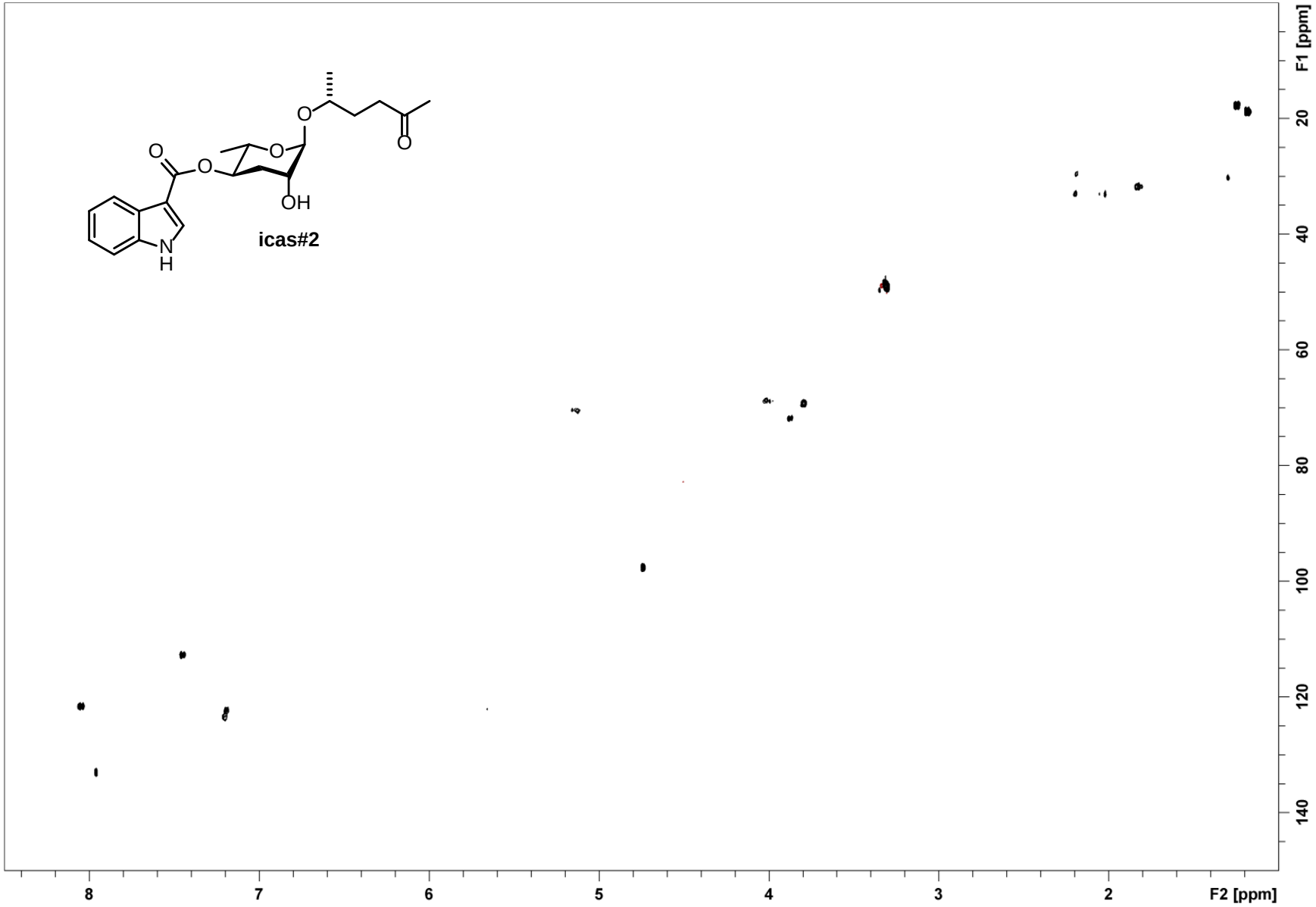

Figure S16: *dqf*-COSY spectrum of icas#2 (**6**) (in $CDCl_3$) isolated from the *C. briggsae* AF16 *exo*-metabolome.

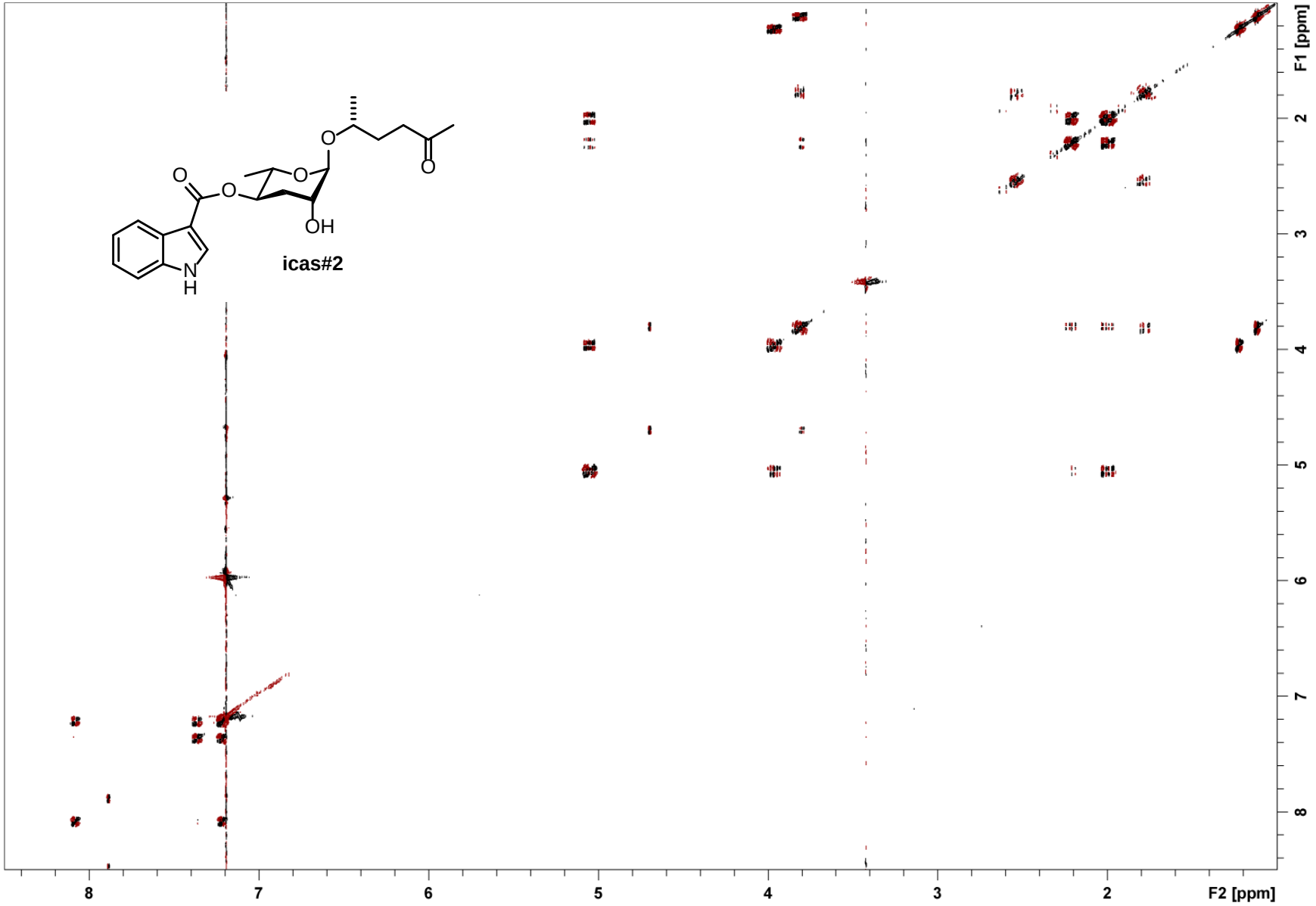

Figure S17: ^{1}H NMR spectrum of (*S*)-icas#6.2 (**7**) (in CD_3OD) isolated from the *C. briggsae* AF16 *exo*-metabolome.

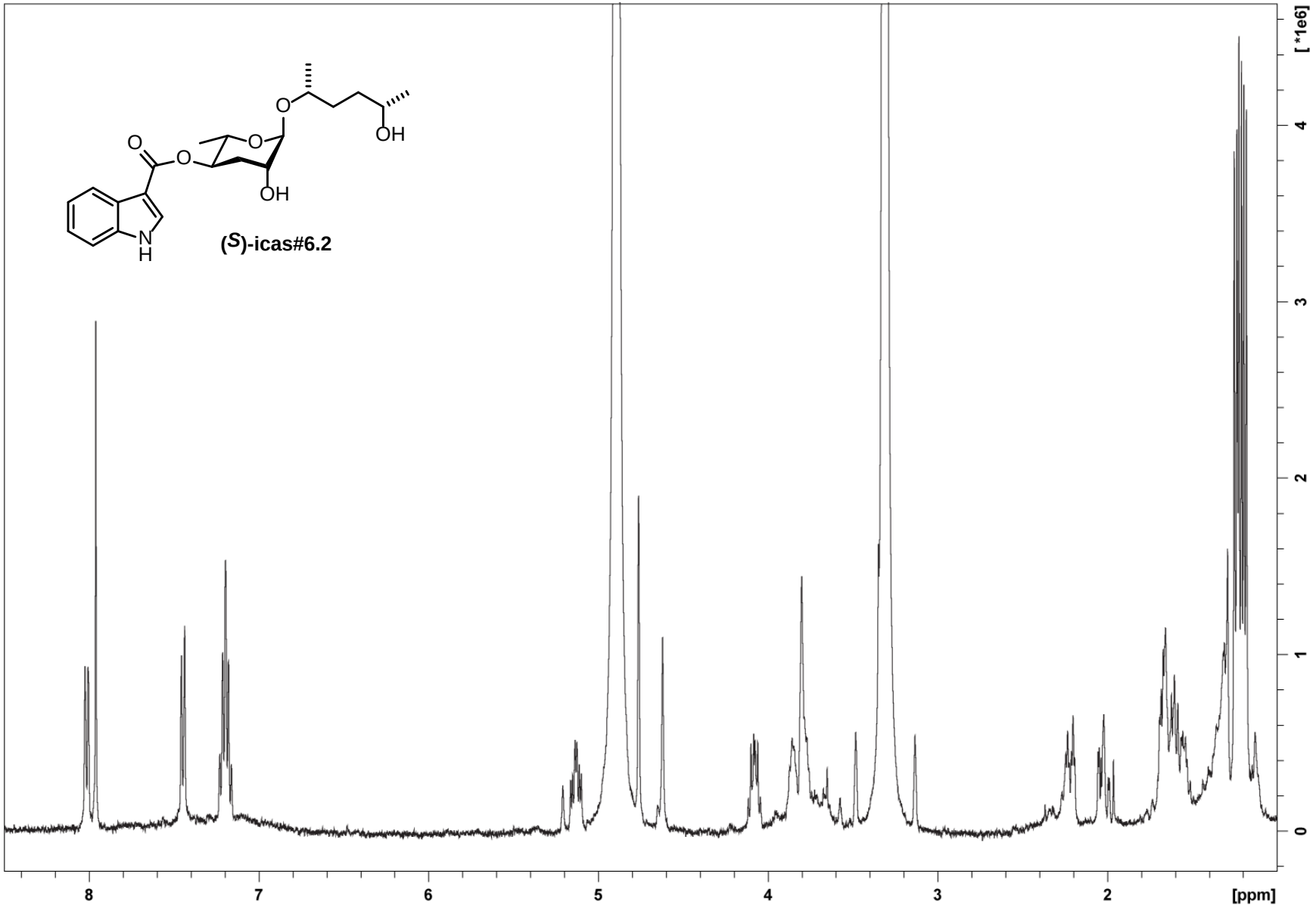

Figure S18: *dqf*-COSY spectrum of (*S*)-icas#6.2 (**7**) (in CD_3OD) isolated from the *C. briggsae* AF16 *exo*-metabolome.

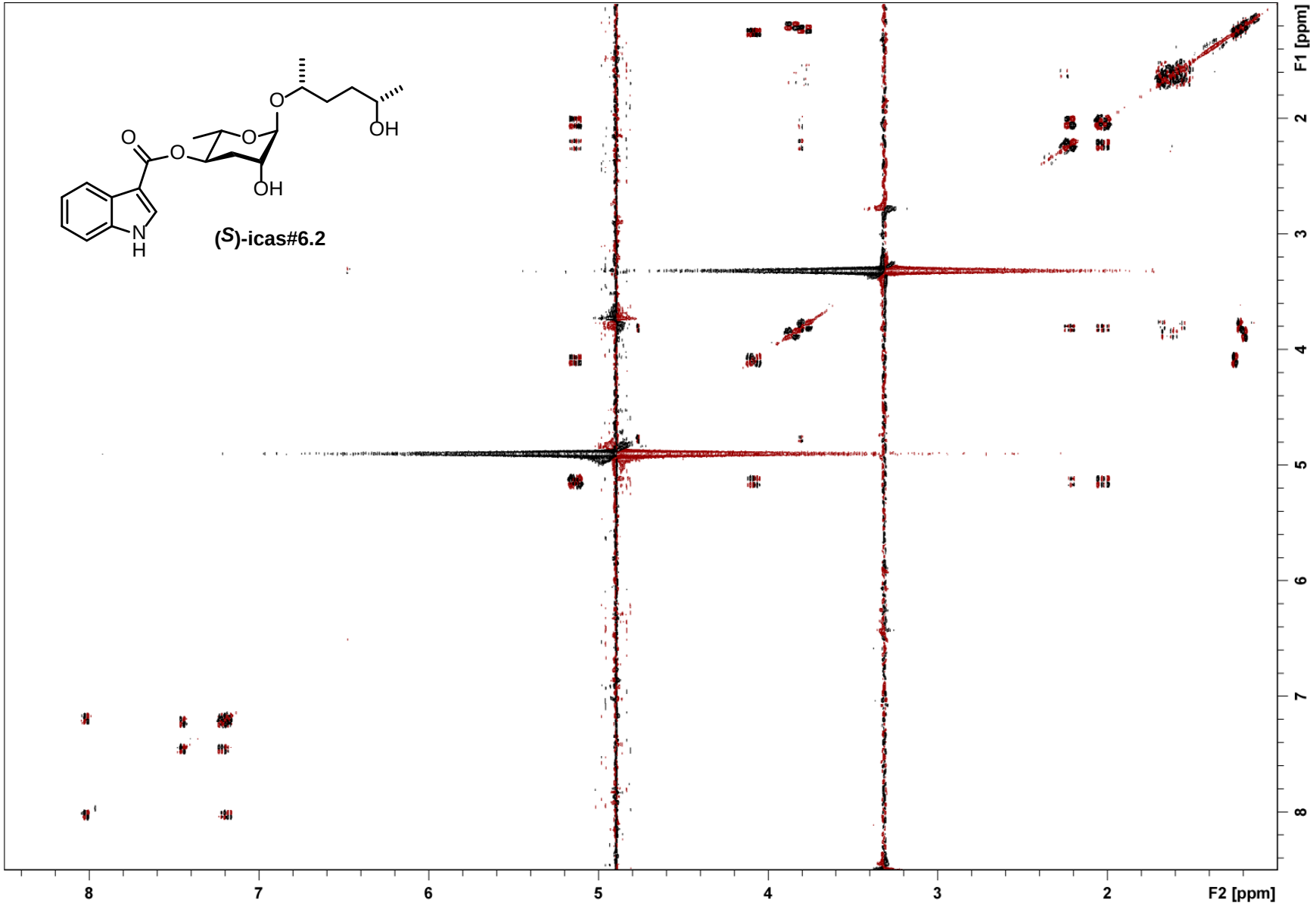

Figure S19: HSQC spectrum of (*S*)-icas#6.2 (**7**) (in CD_3OD) isolated from the *C. briggsae* AF16 *exo*-metabolome.

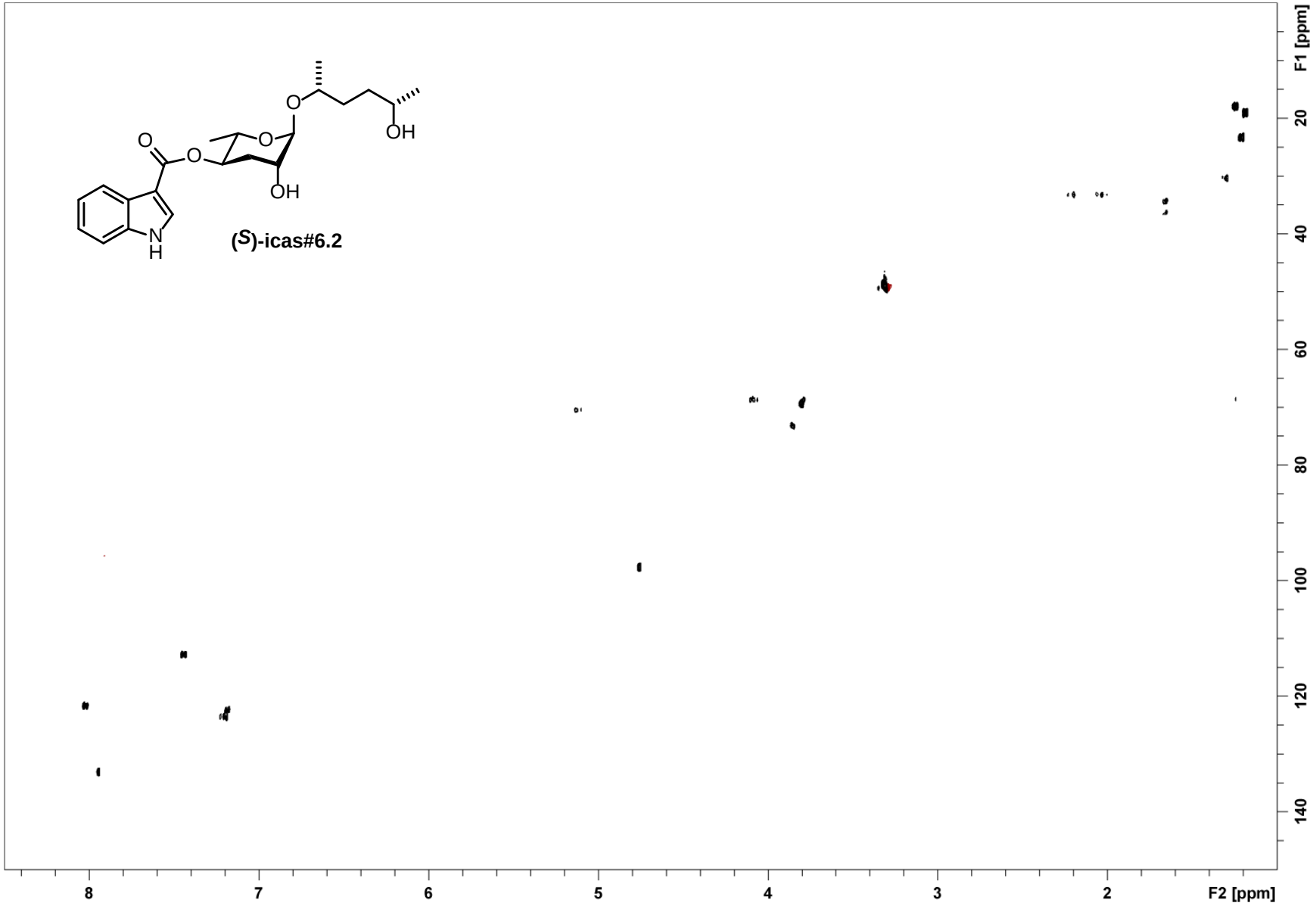

FigureS20: ^{1}H NMR spectrum of synthetic 2,4-di-*O*-benzoyl-ascr#6.1 (**8**) (in CD_3OD).

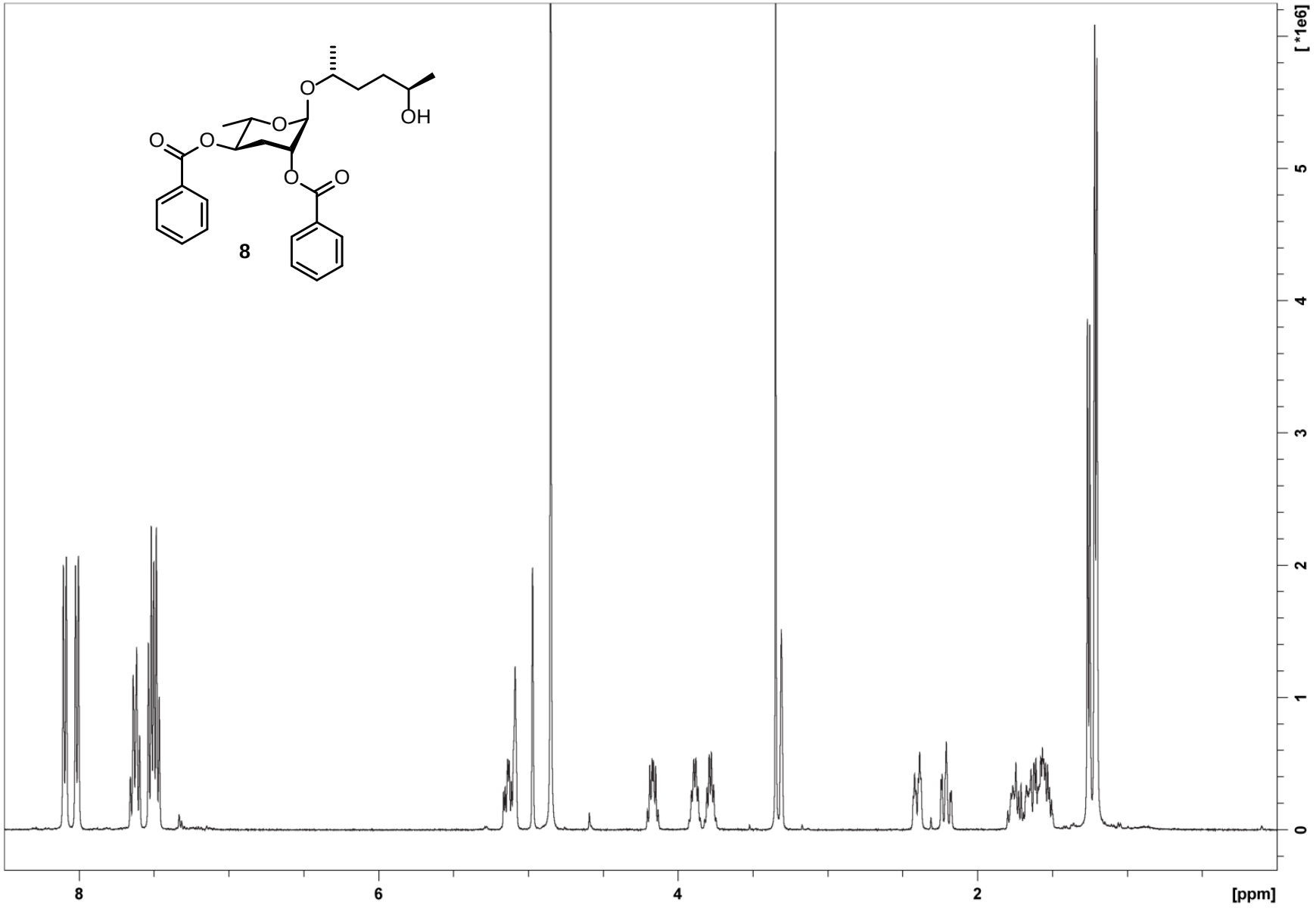

Figure S21: ^{13}C NMR spectrum of synthetic 2,4-di-*O*-benzoyl-ascr#6.1 (**8**) (in CD_3OD).

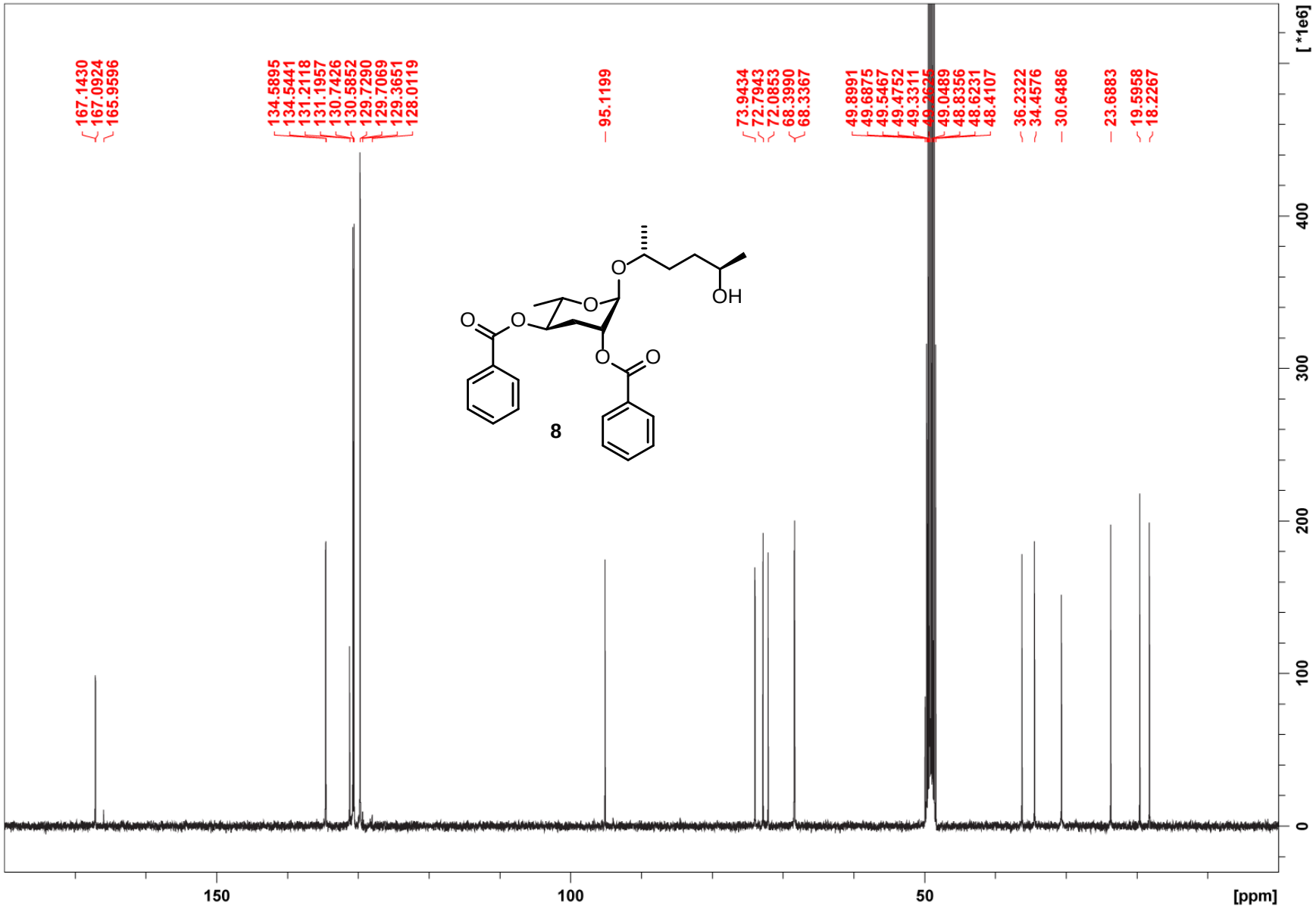

Figure S22: ^{1}H NMR spectrum of synthetic 2,4-di-*O*-benzoyl-ascr#2 (**9**) (in $CDCl_3$).

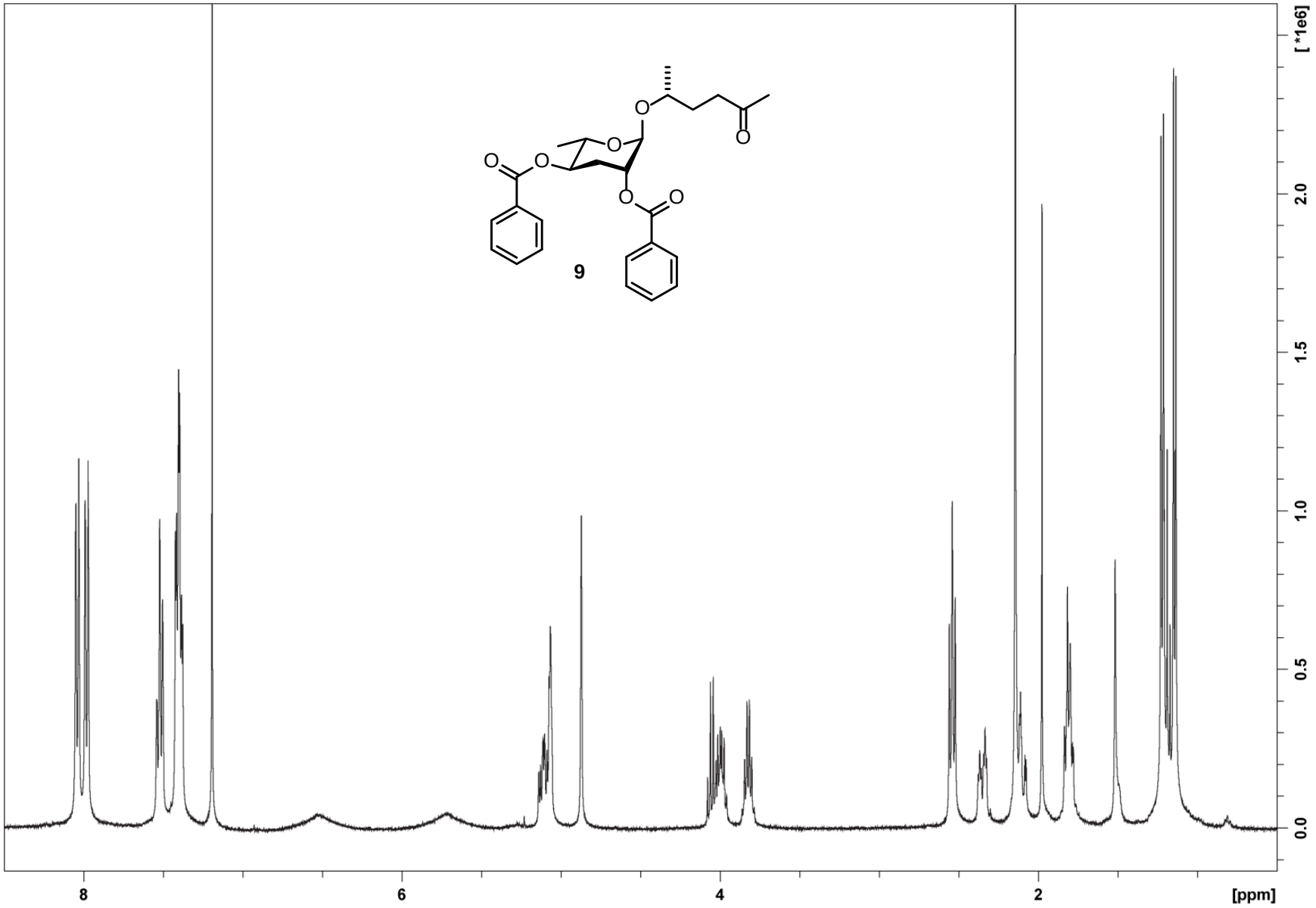

Figure S23: ^{1}H NMR spectrum of synthetic ascr#2 (**2**) (in CD_3OD).

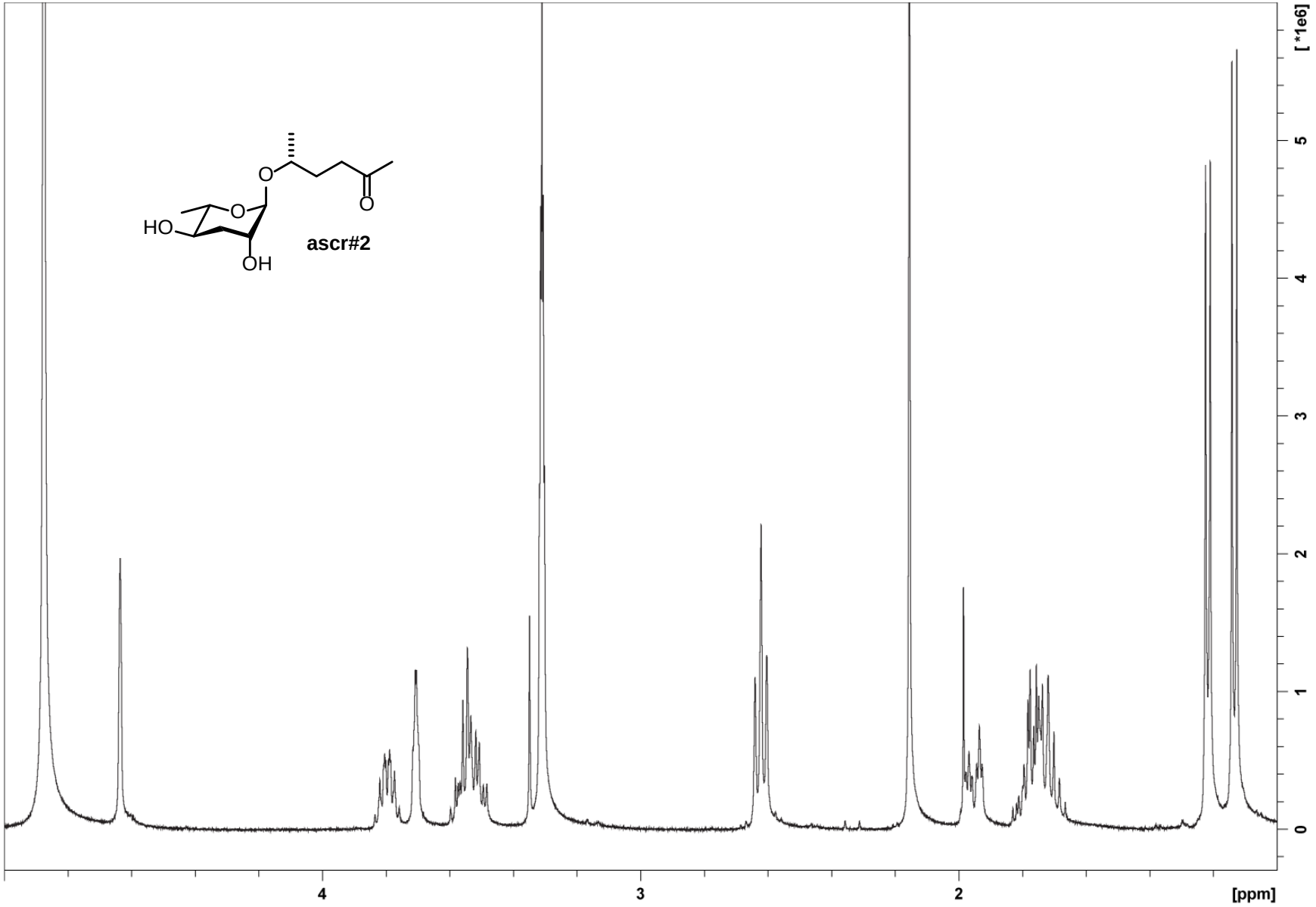

Figure S24: ^{13}C NMR spectrum of synthetic ascr#2 (**2**) (in CD_3OD).

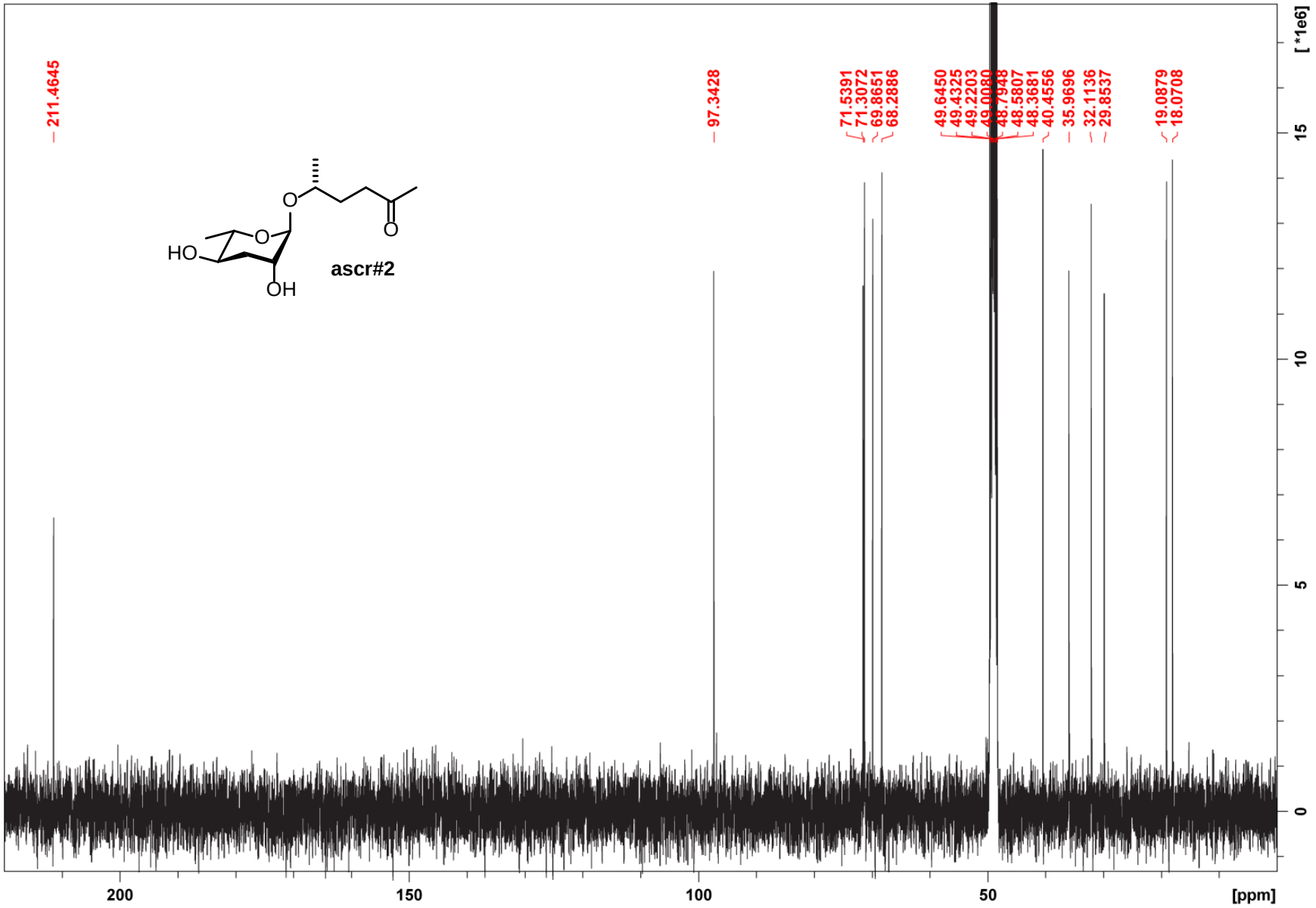

Figure S25: ^{1}H NMR spectrum of synthetic 2,4-di-*O*-(indole-3-carbonyl)-ascr#2 (**10**) (in CD_3OD).

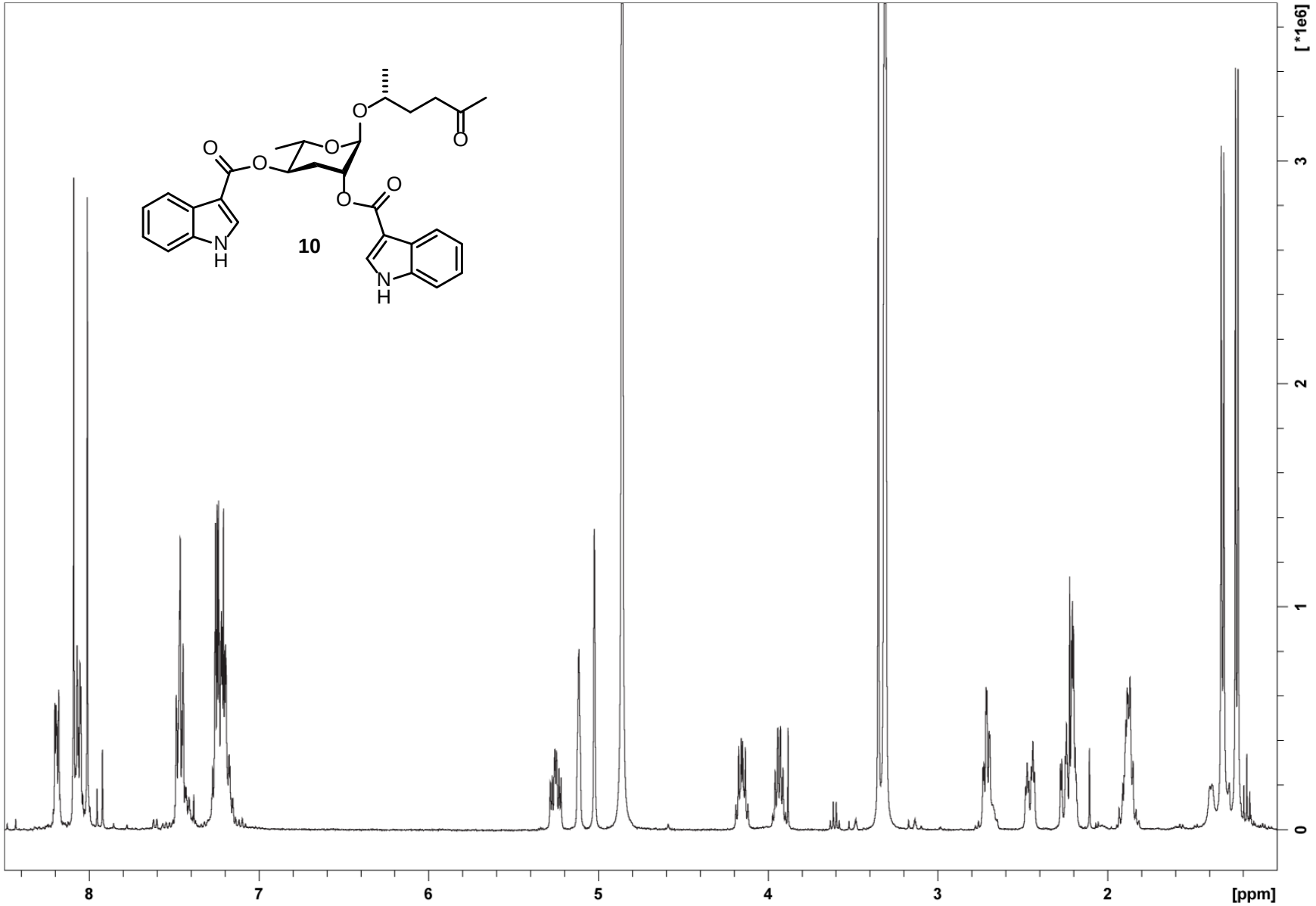

Figure S26: ^{13}C NMR spectrum of synthetic 2,4-di-*O*-(indole-3-carbonyl)-ascr#2 (**10**) (in CD_3OD).

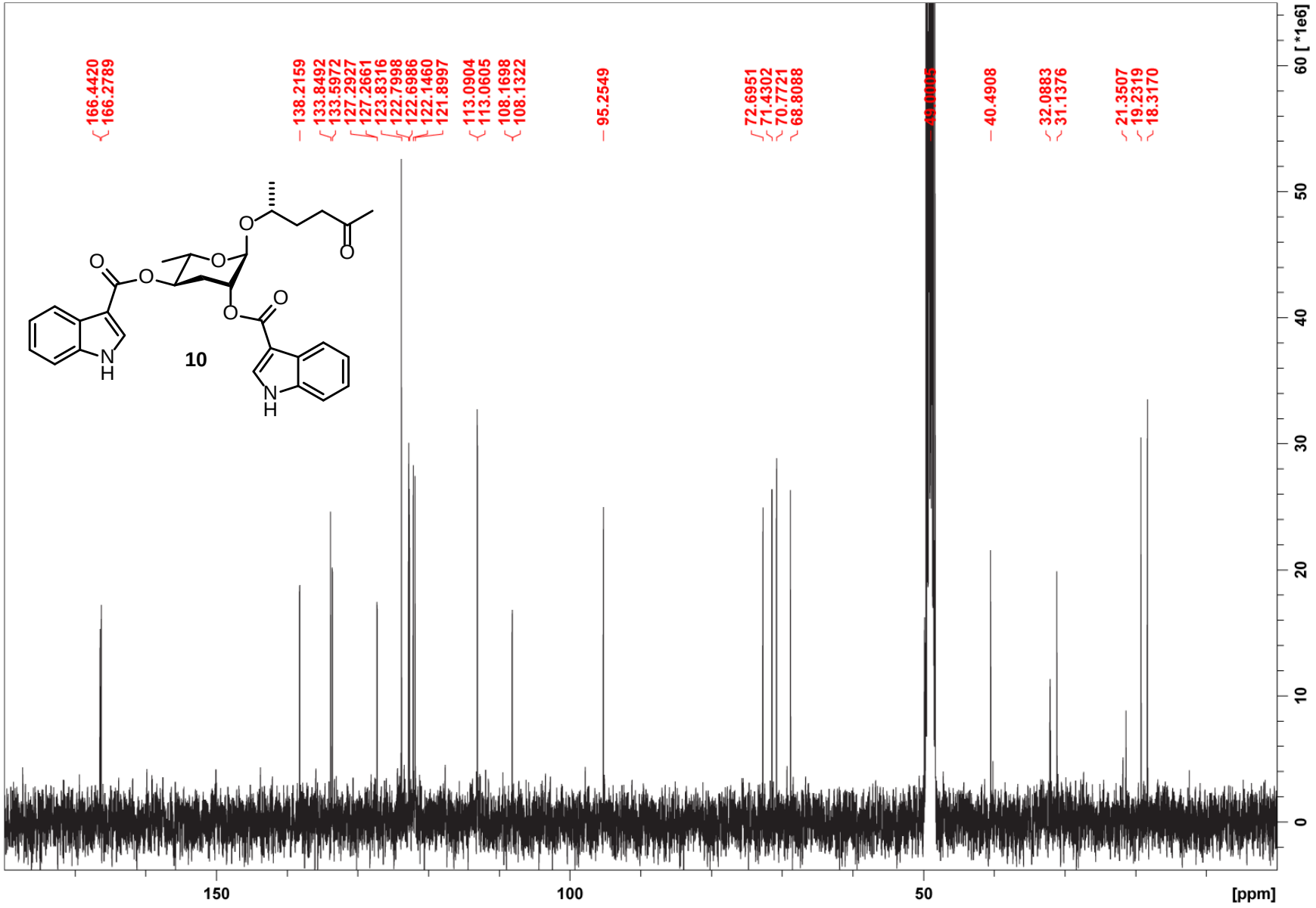

Figure S27: *dqf*-COSY spectrum of synthetic 2,4-di-*O*-(indole-3-carbonyl)-ascr#2 (**10**) (in CD_3OD).

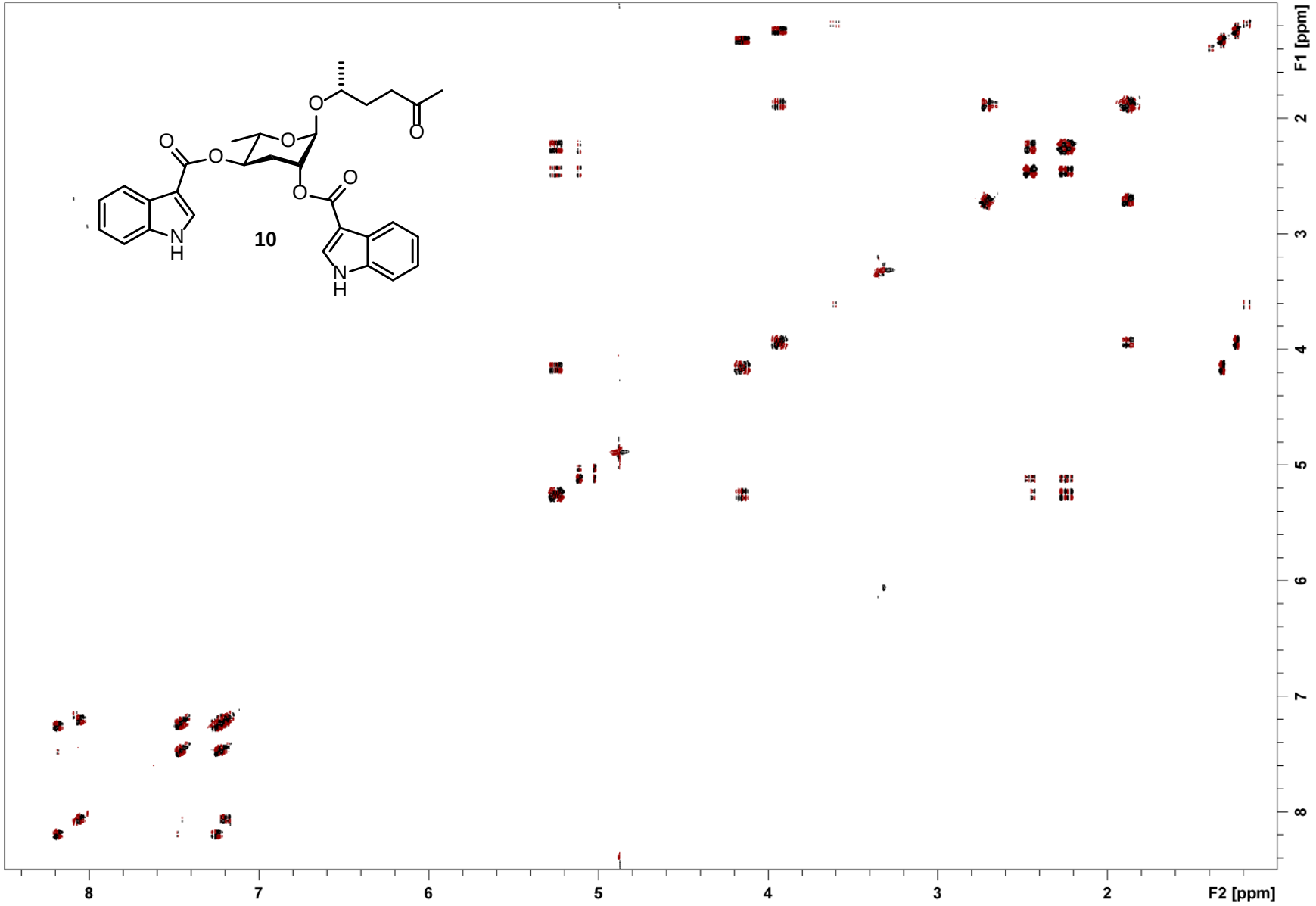

Figure S28: HSQC spectrum of synthetic 2,4-di-*O*-(indole-3-carbonyl)-ascr#2 (**10**) (in CD_3OD).

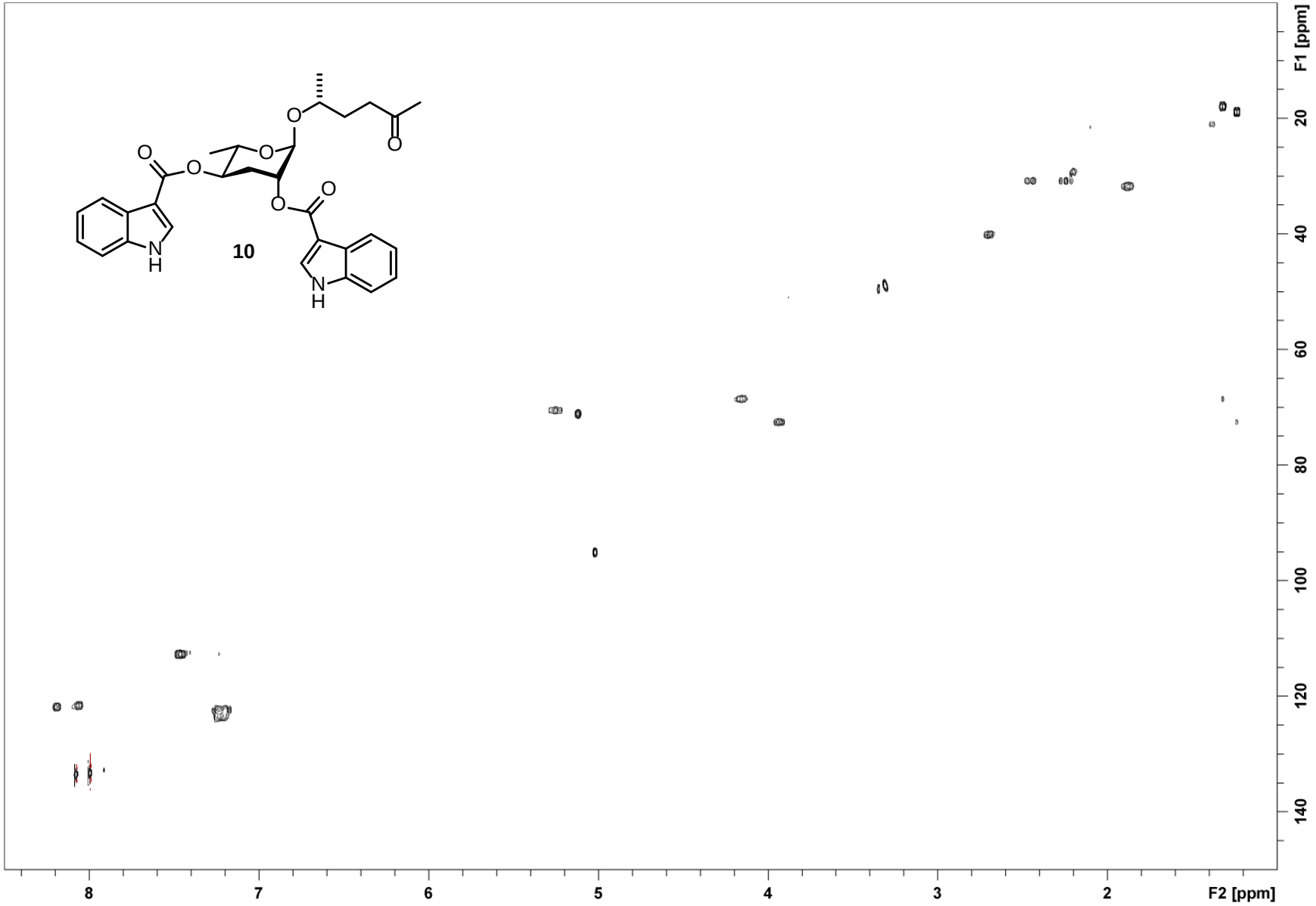

Figure S29: ^{1}H NMR spectra of natural icas#2 (**6**) isolated from the *C. briggsae* AF16 *exo*-metabolome (A) and synthetic icas#2 (B) in CD_3OD.

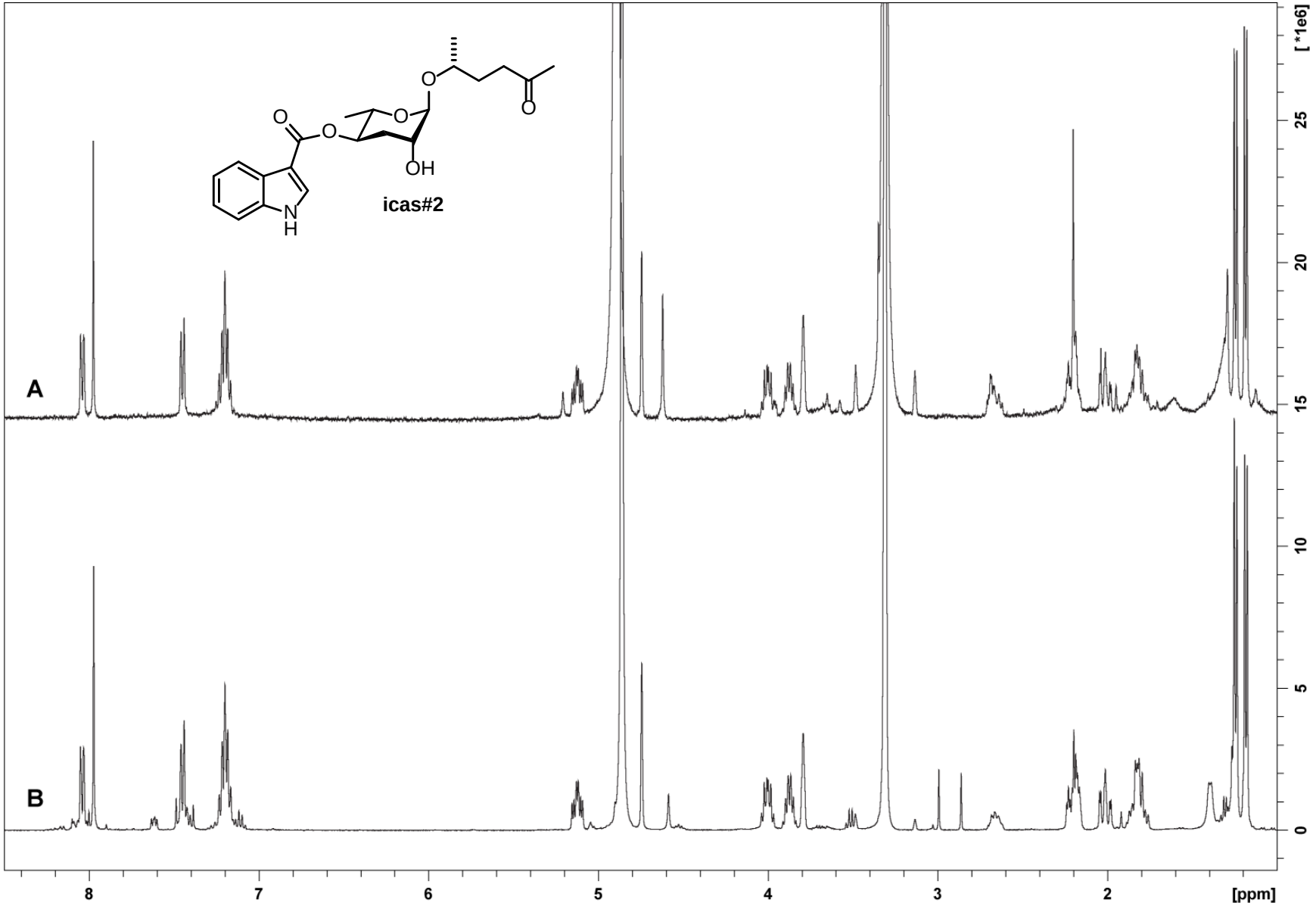

Figure S30: ^{1}H NMR spectrum of synthetic icas#2 (**6**) (in CD_3OD).

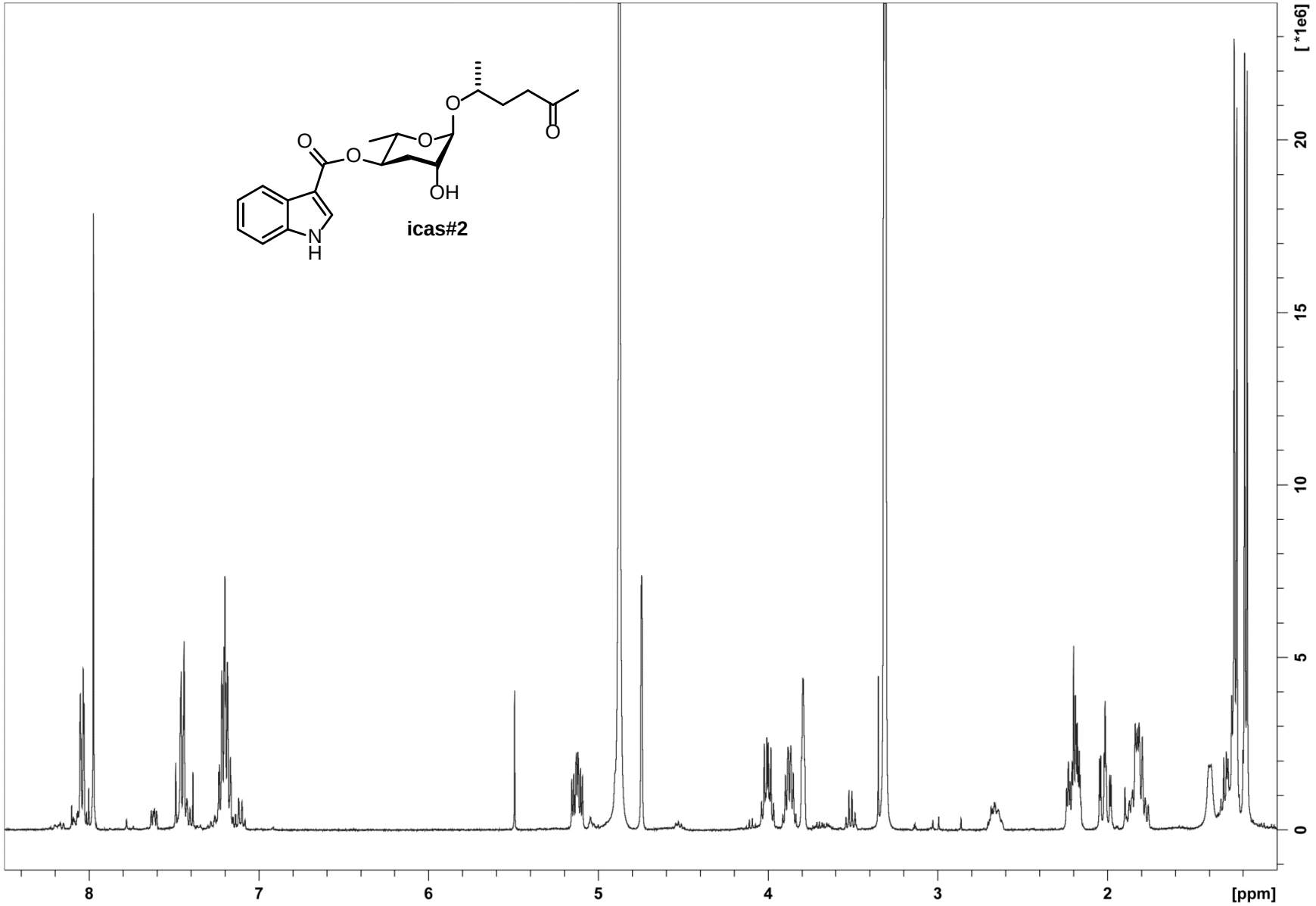

Figure S31: *dqf*-COSY spectrum of synthetic icas#2 (**6**) (in CD_3OD).

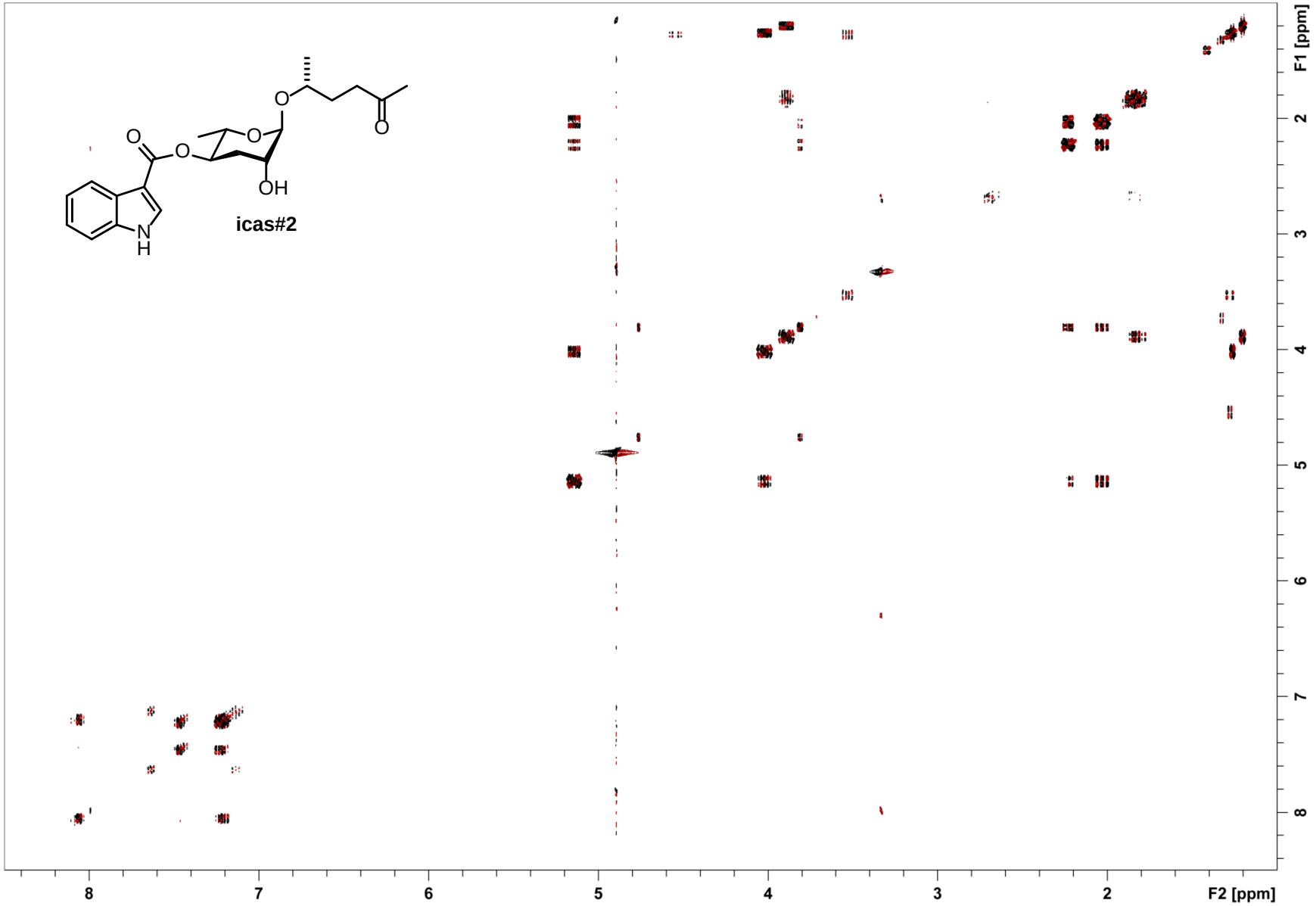

Figure S32: HSQC spectrum of synthetic icas#2 (**6**) (in CD_3OD).

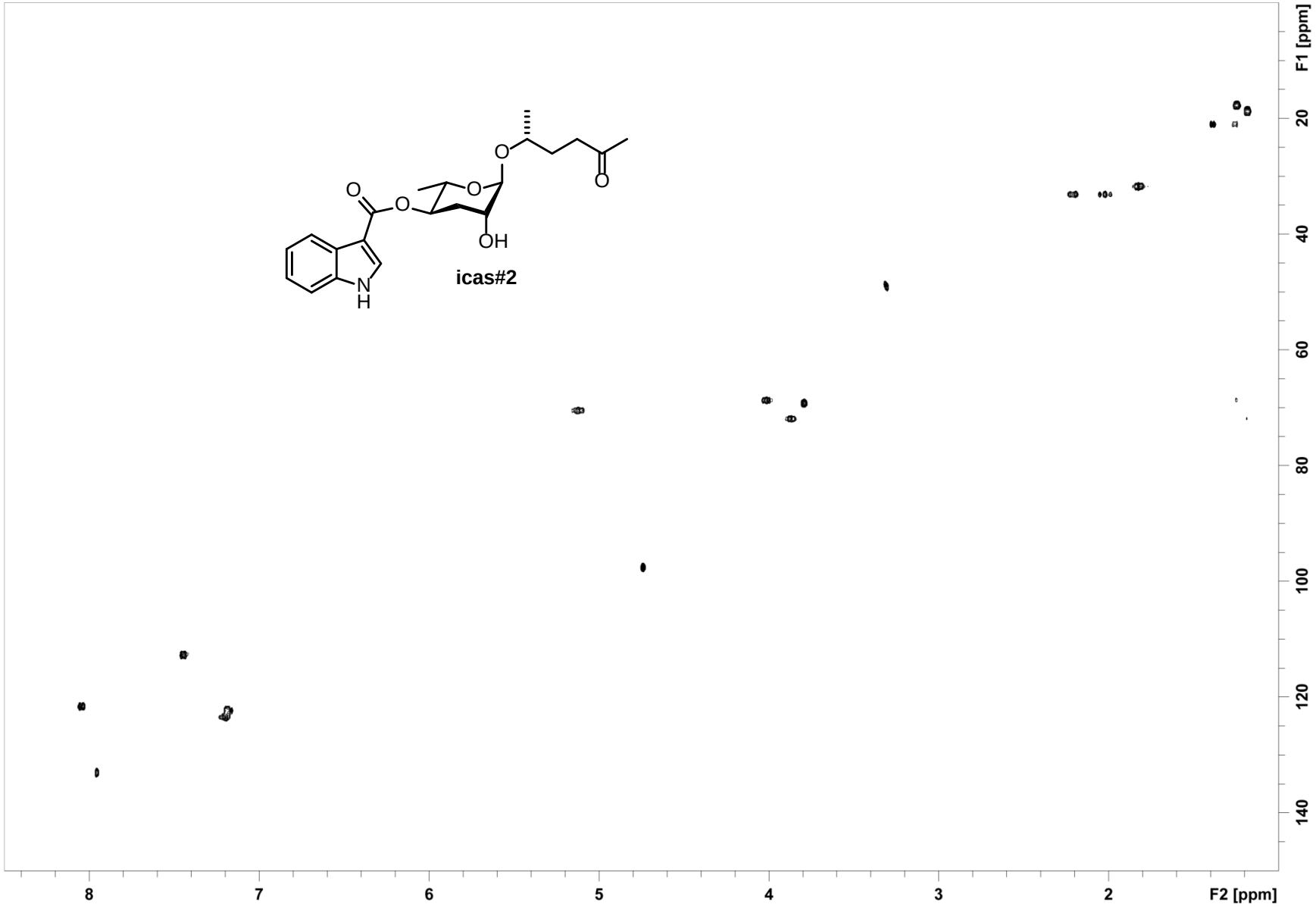

Figure S33: ^{1}H NMR spectrum of synthetic 2,4-di-*O*-benzoyl-2'-*O*-TBS-ascr#6.1 (**11**) (in $CDCl_3$).

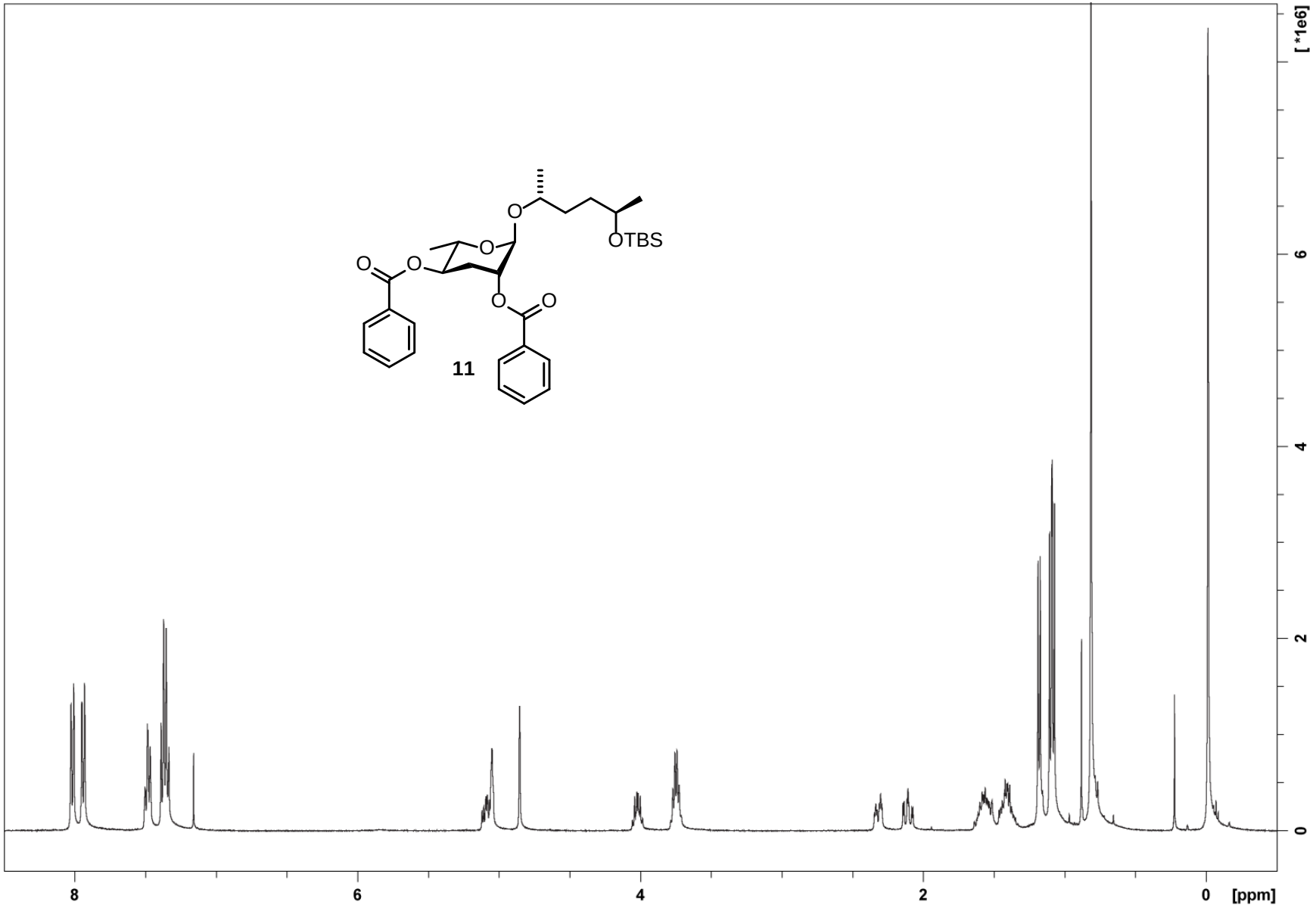

Figure S34: ^{13}C NMR spectrum of synthetic 2,4-di-*O*-benzoyl-2'-*O*-TBS-ascr#6.1 (**11**) (in $CDCl_3$).

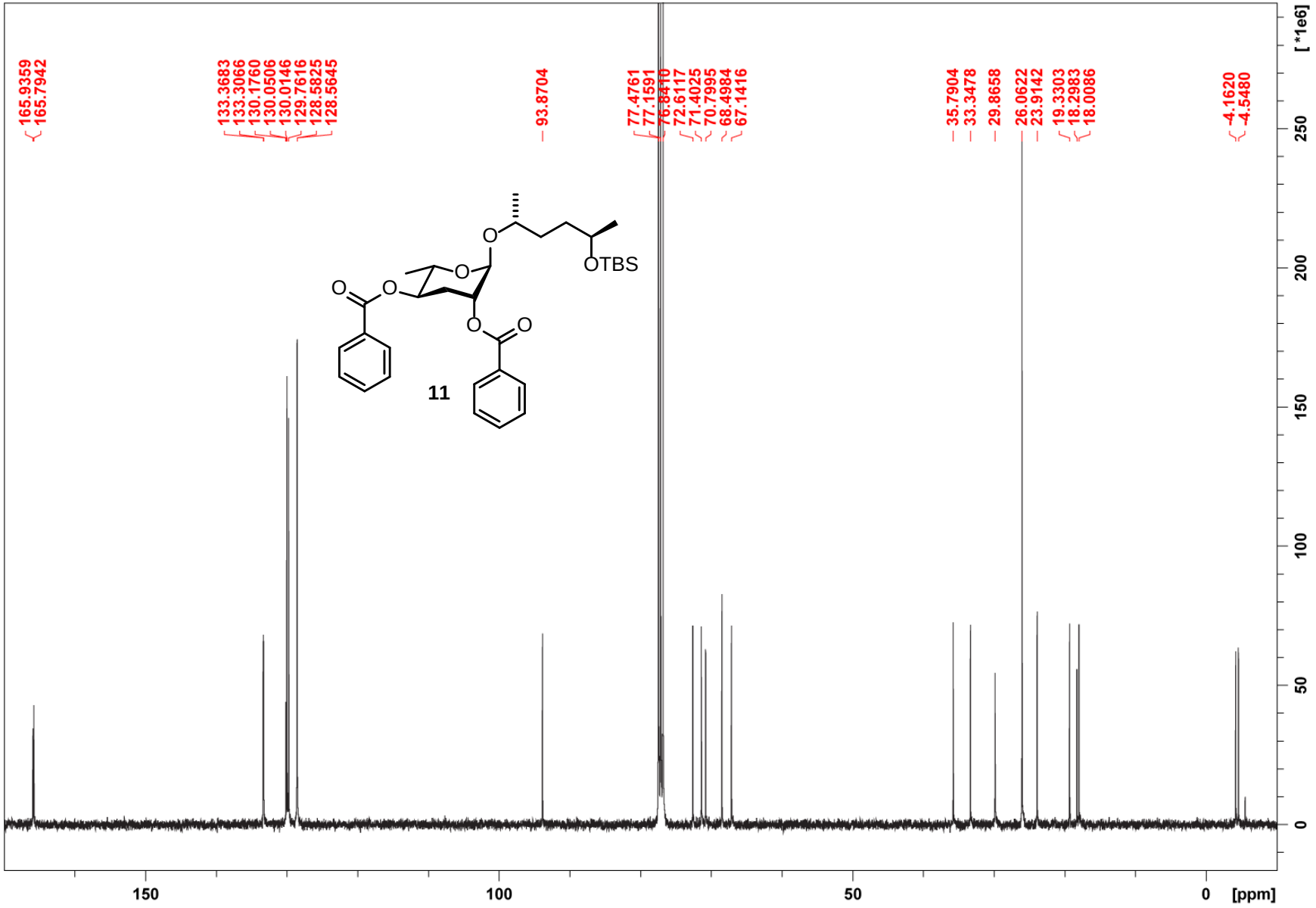

Figure S35: ^{1}H NMR spectrum of synthetic 2'-*O*-TBS-ascr#6.1 (**12**) (in CD_3OD).

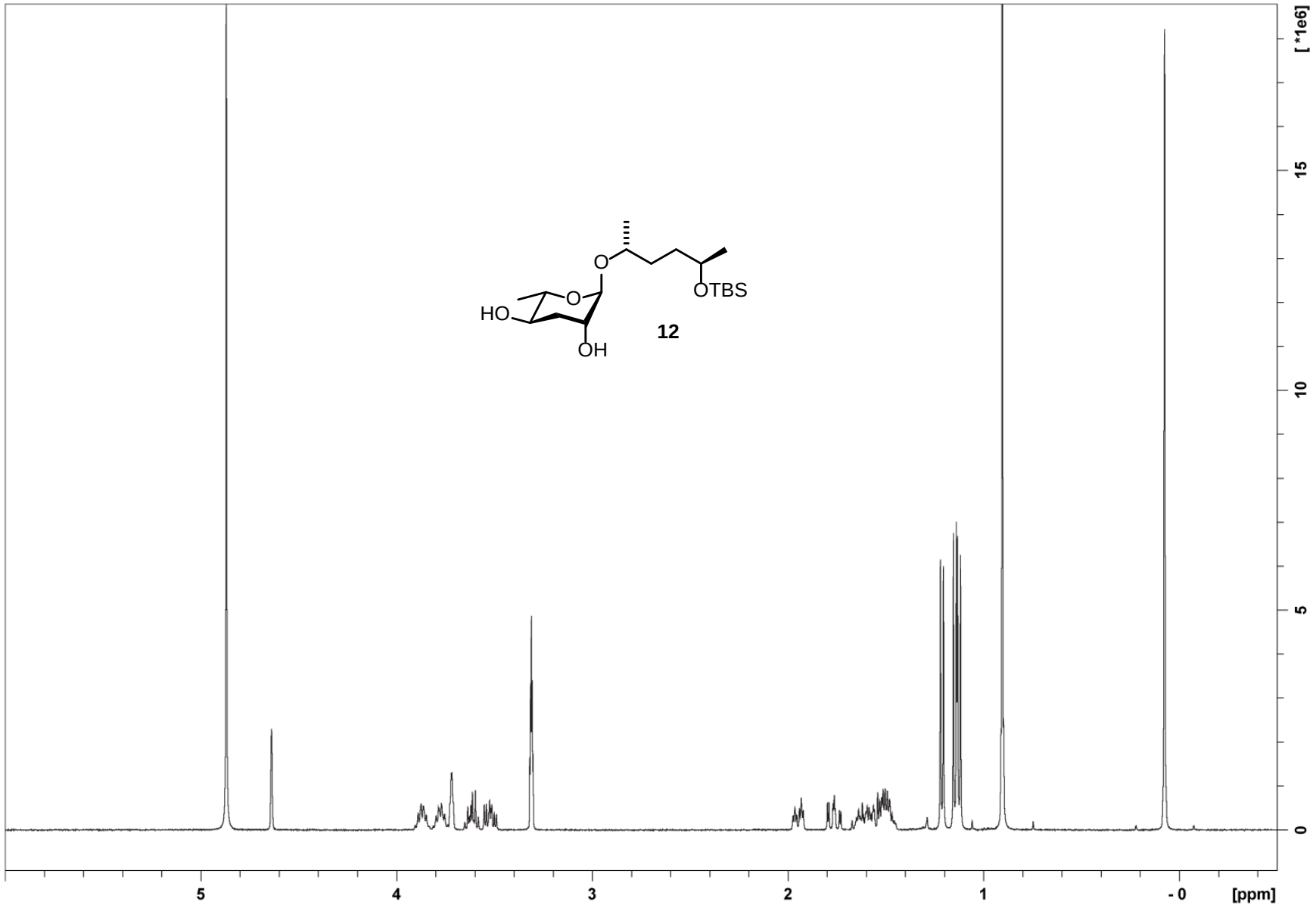

Figure S36: *dqf*-COSY spectrum of synthetic 2'-*O*-TBS-ascr#6.1 (**12**) (in CD_3OD).

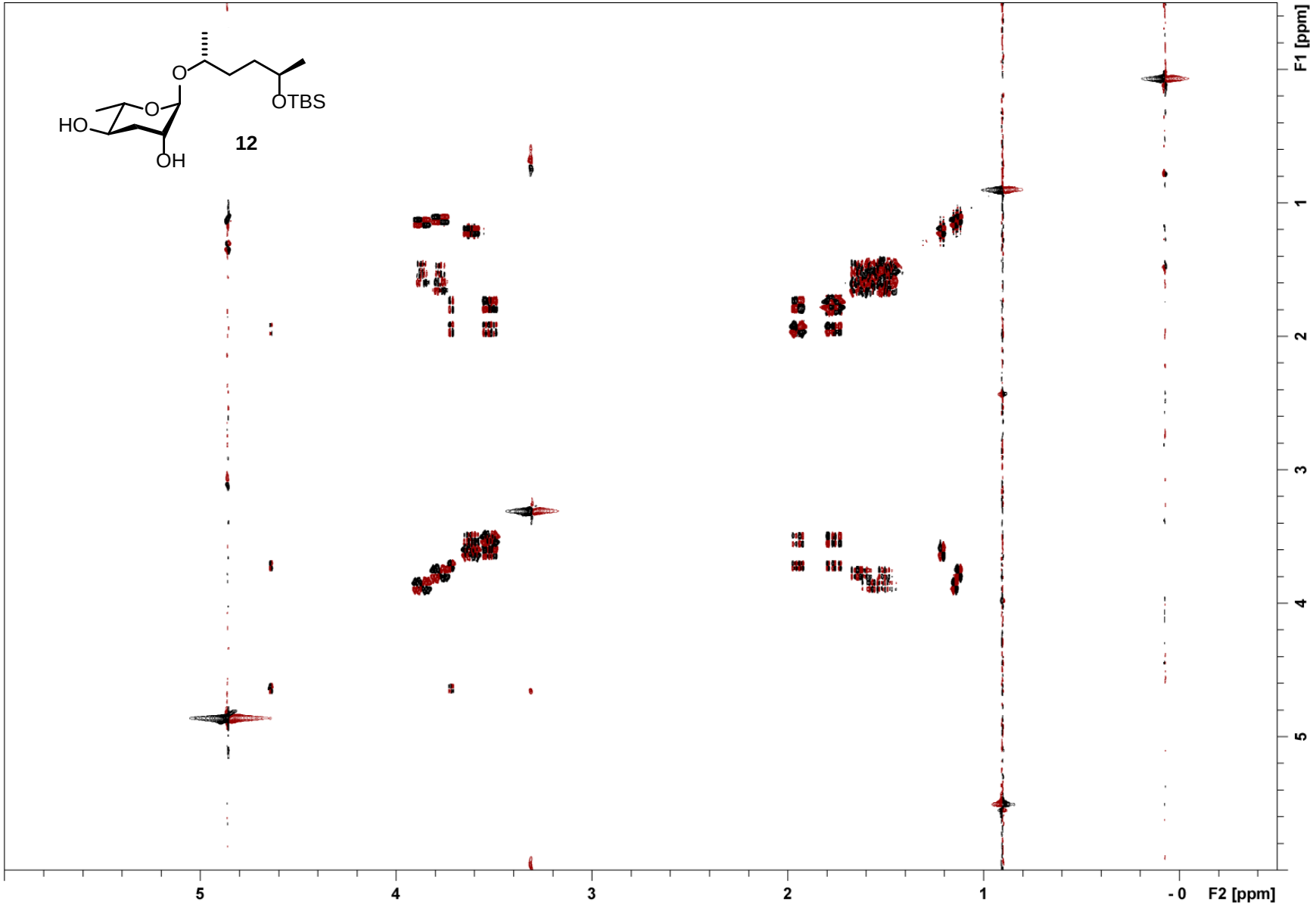

Figure S37: HSQC spectrum of synthetic 2'-*O*-TBS-ascr#6.1 (**12**) (in CD_3OD).

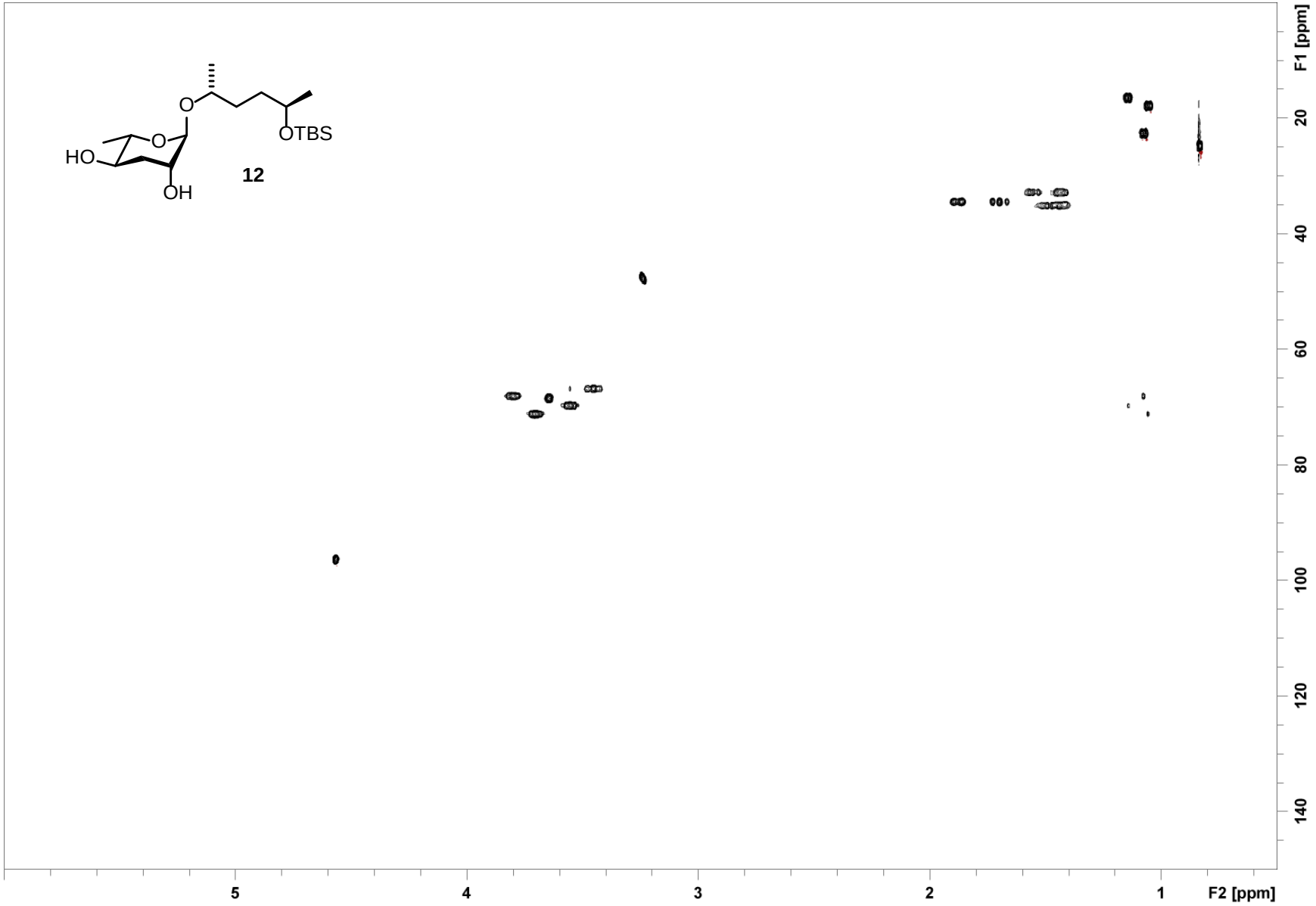

Figure S38: ^{1}H NMR spectrum of synthetic 4-*O*-(indole-3-carbonyl)-2'-*O*-TBS-ascr#6.1 (**13**) (in CD_3OD).

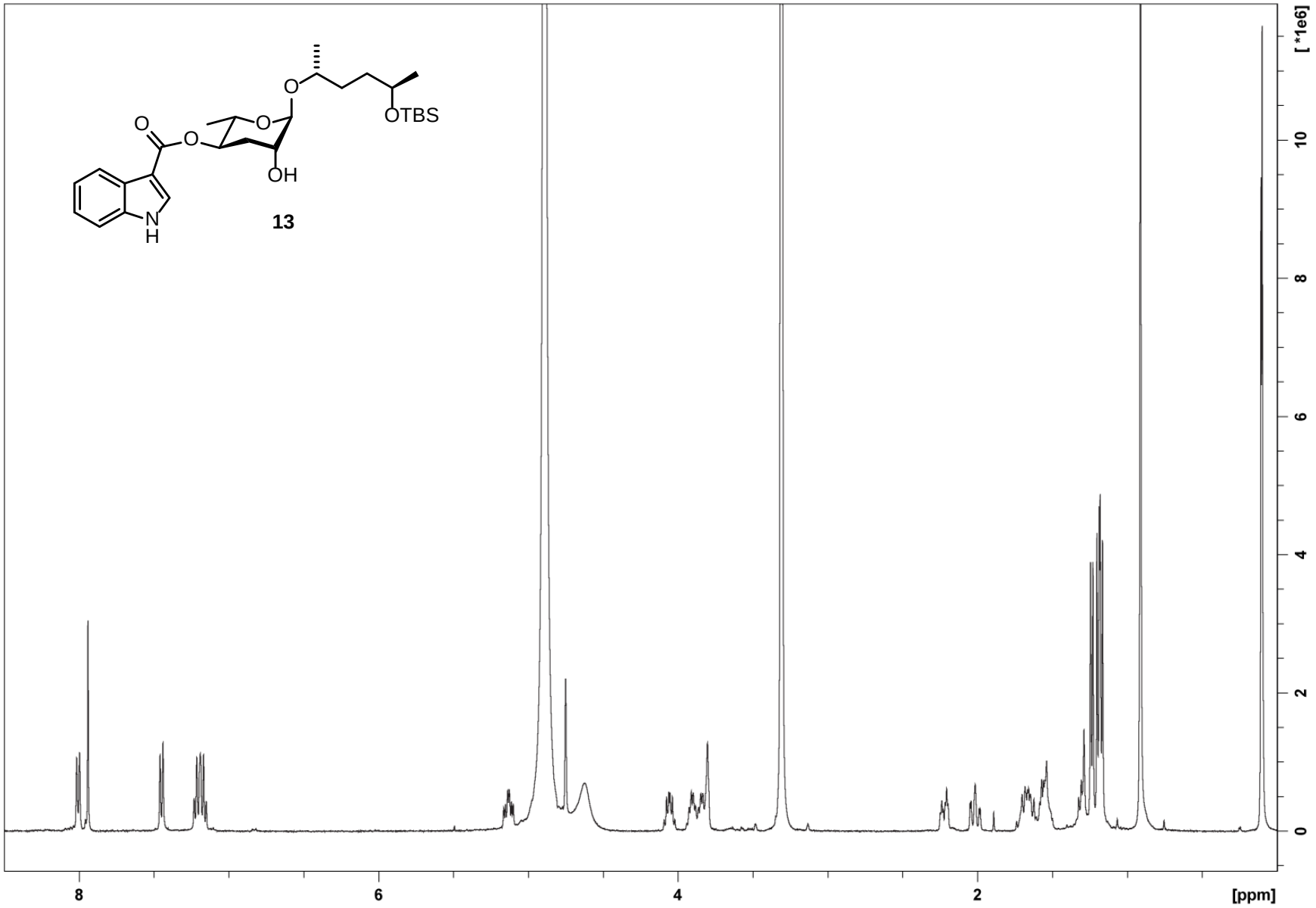

Figure S39: *dqf*-COSY spectrum of synthetic 4-*O*-(indole-3-carbonyl)-2'-*O*-TBS-ascr#6.1 (**13**) (in CD_3OD).

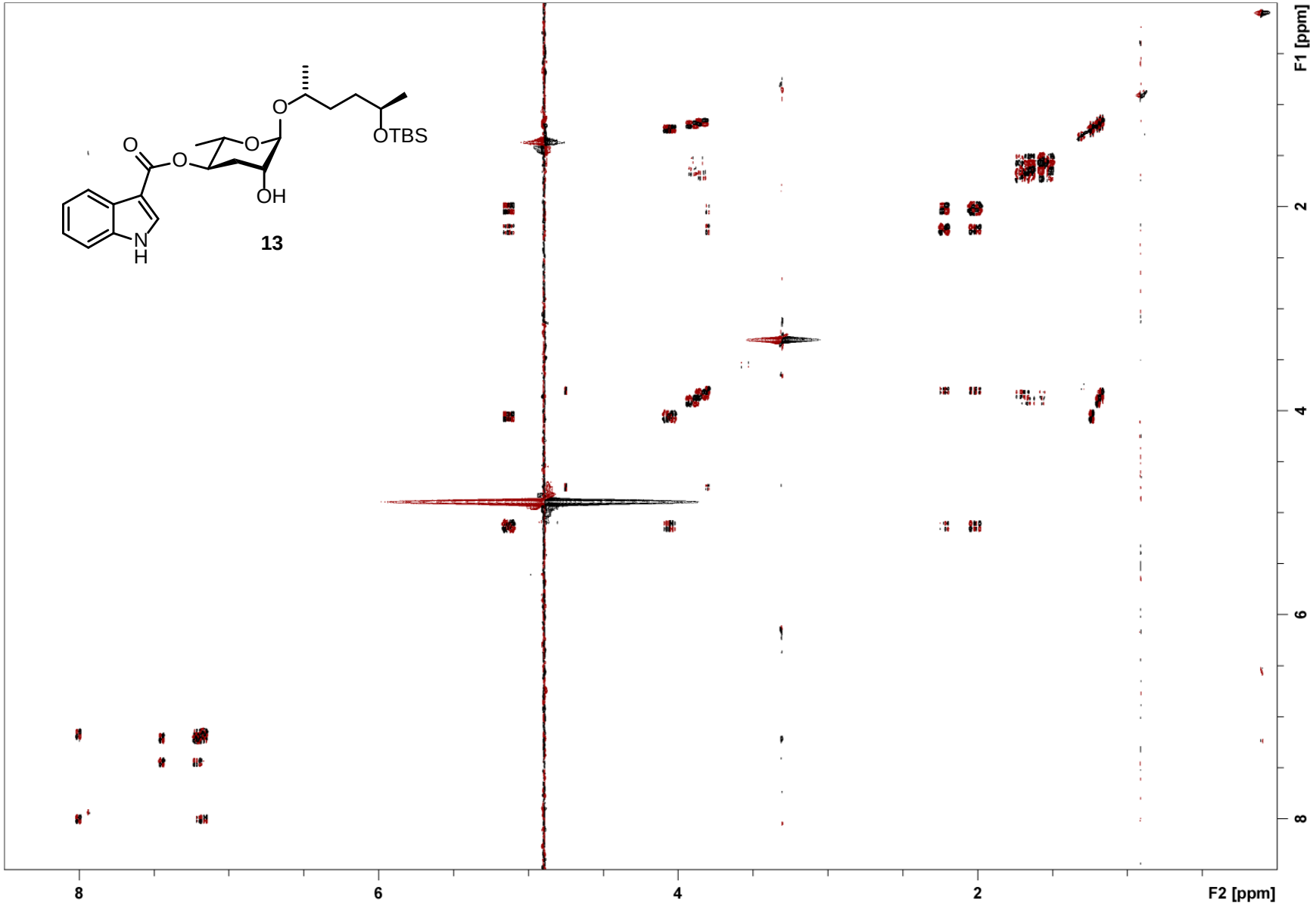

Figure S40: HSQC spectrum of synthetic 4-*O*-(indole-3-carbonyl)-2'-*O*-TBS-ascr#6.1 (**13**) (in CD_3OD).

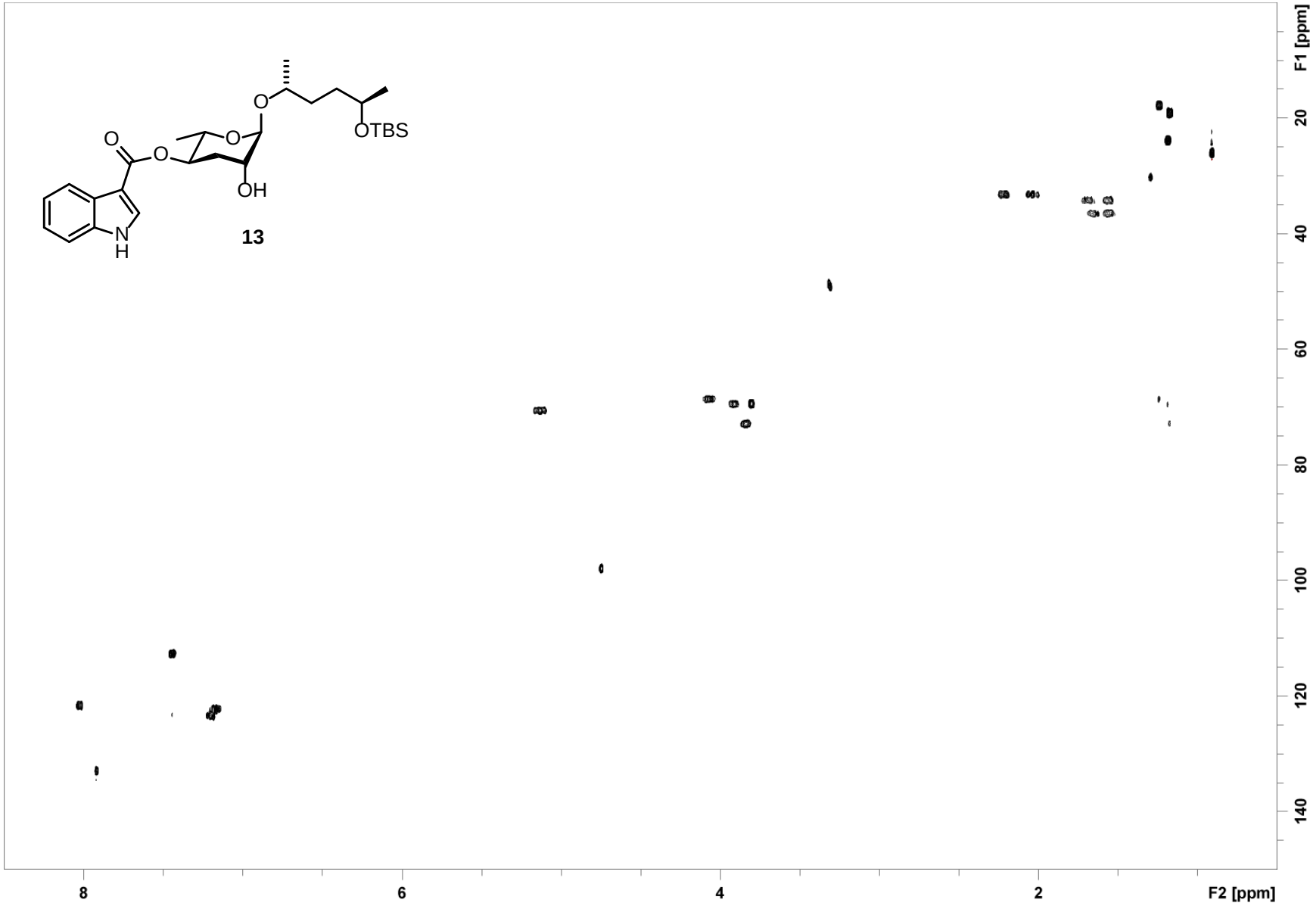

Figure S41: ^{1}H NMR spectrum of synthetic (*R*)-icas#6.1 (**14**) (in CD_3OD).

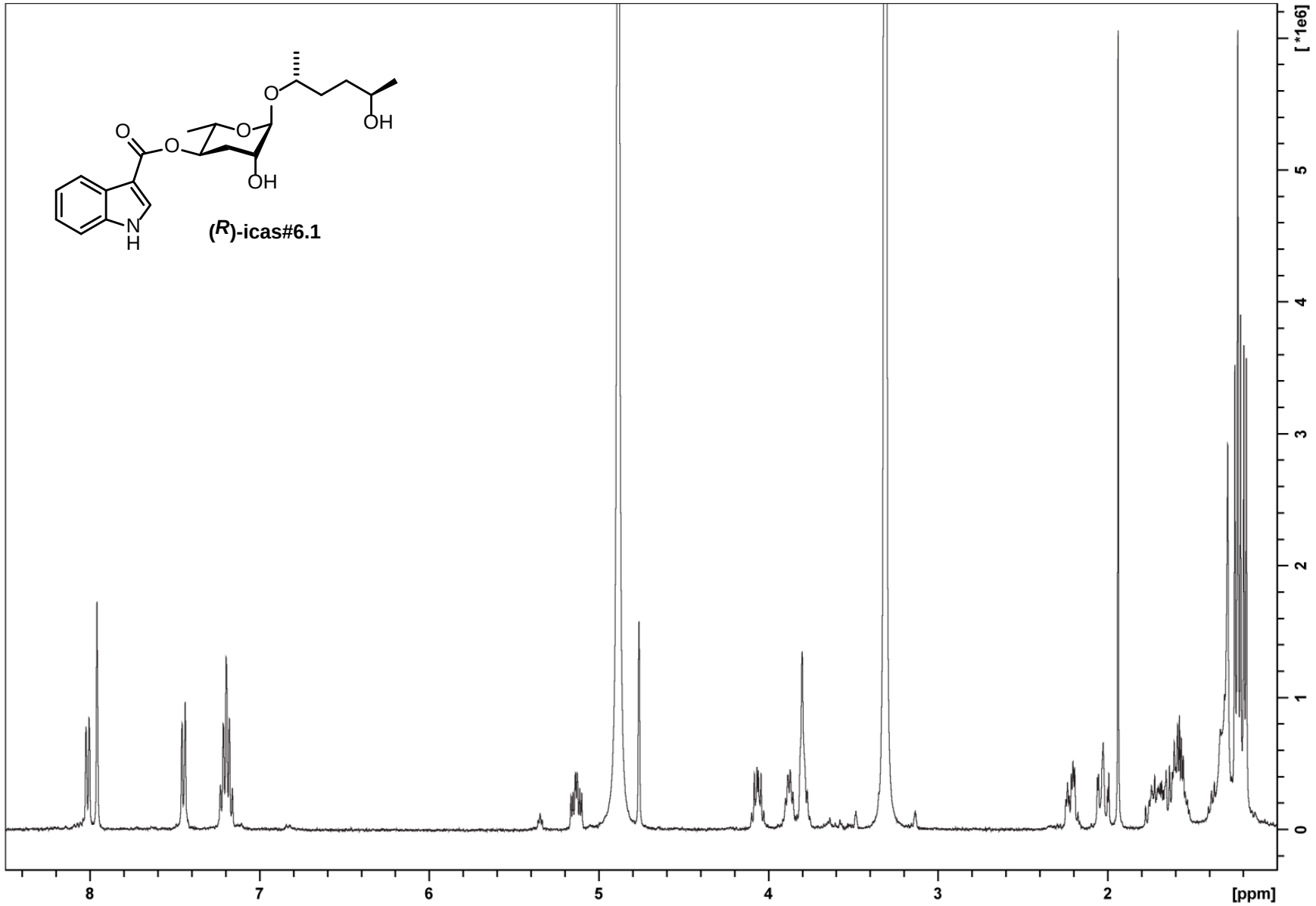

Figure S42: *dqf*-COSY spectrum of synthetic (*R*)-icas#6.1 (**14**) (in CD_3OD).

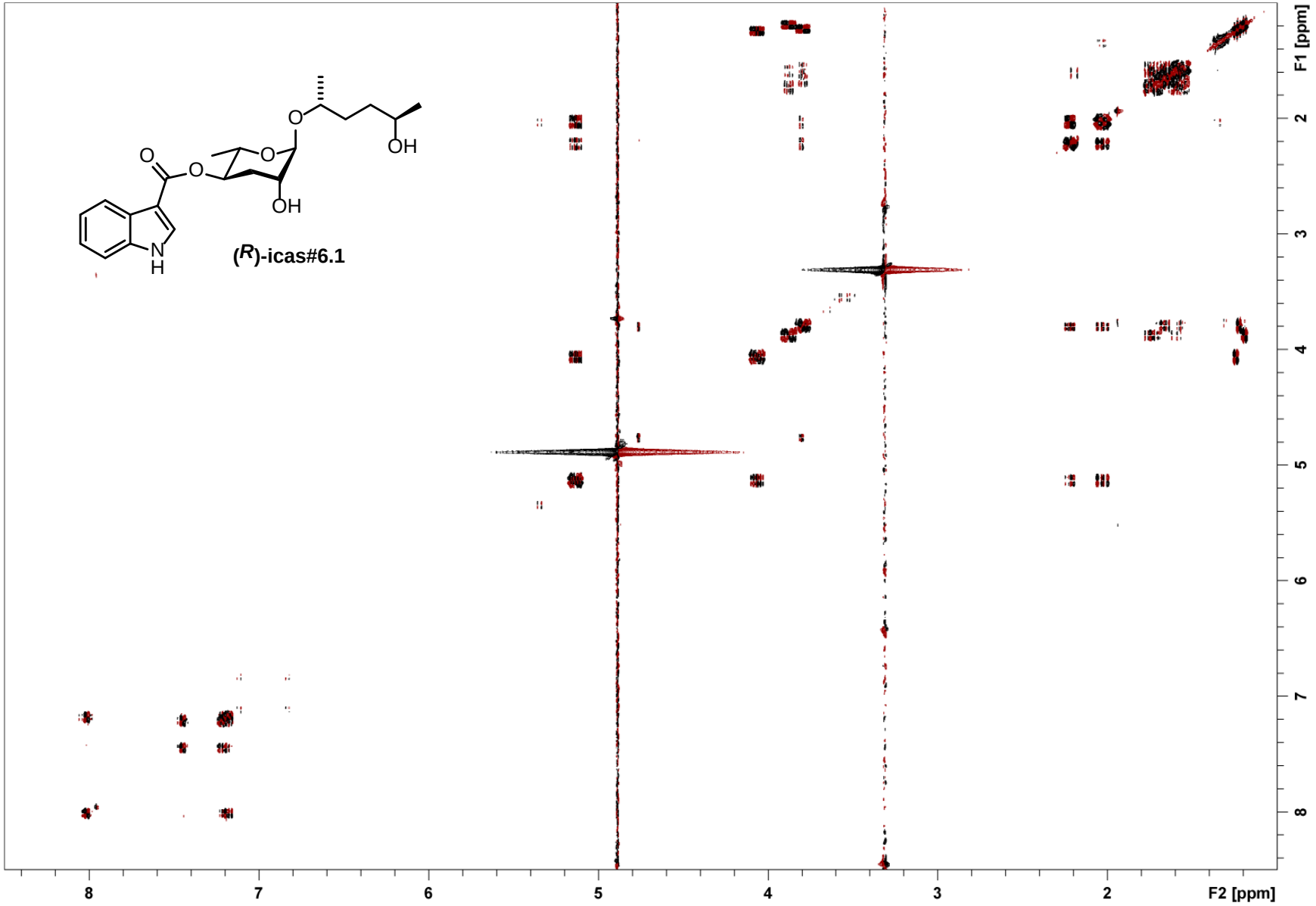

Figure S43: HSQC spectrum of synthetic (*R*)-icas#6.1 (**14**) (in CD_3OD).

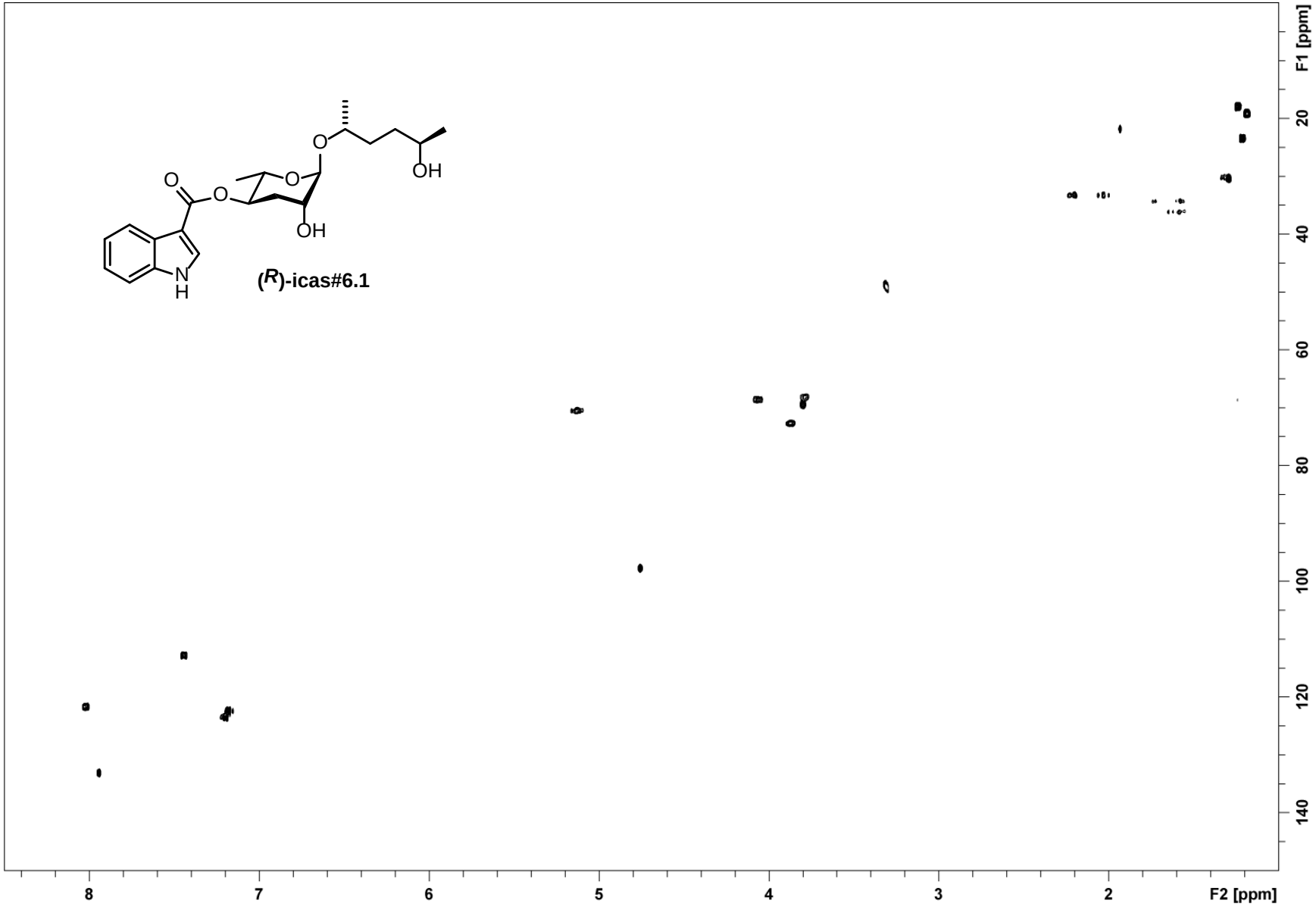

Figure S44: ^{1}H NMR spectra of natural (*S*)-icas#6.2 (**7**) isolated from the *C. briggsae* AF16 *exo*-metabolome (A) and synthetic (*R*)-icas#6.1 (**14**) (B) in CD_3OD.